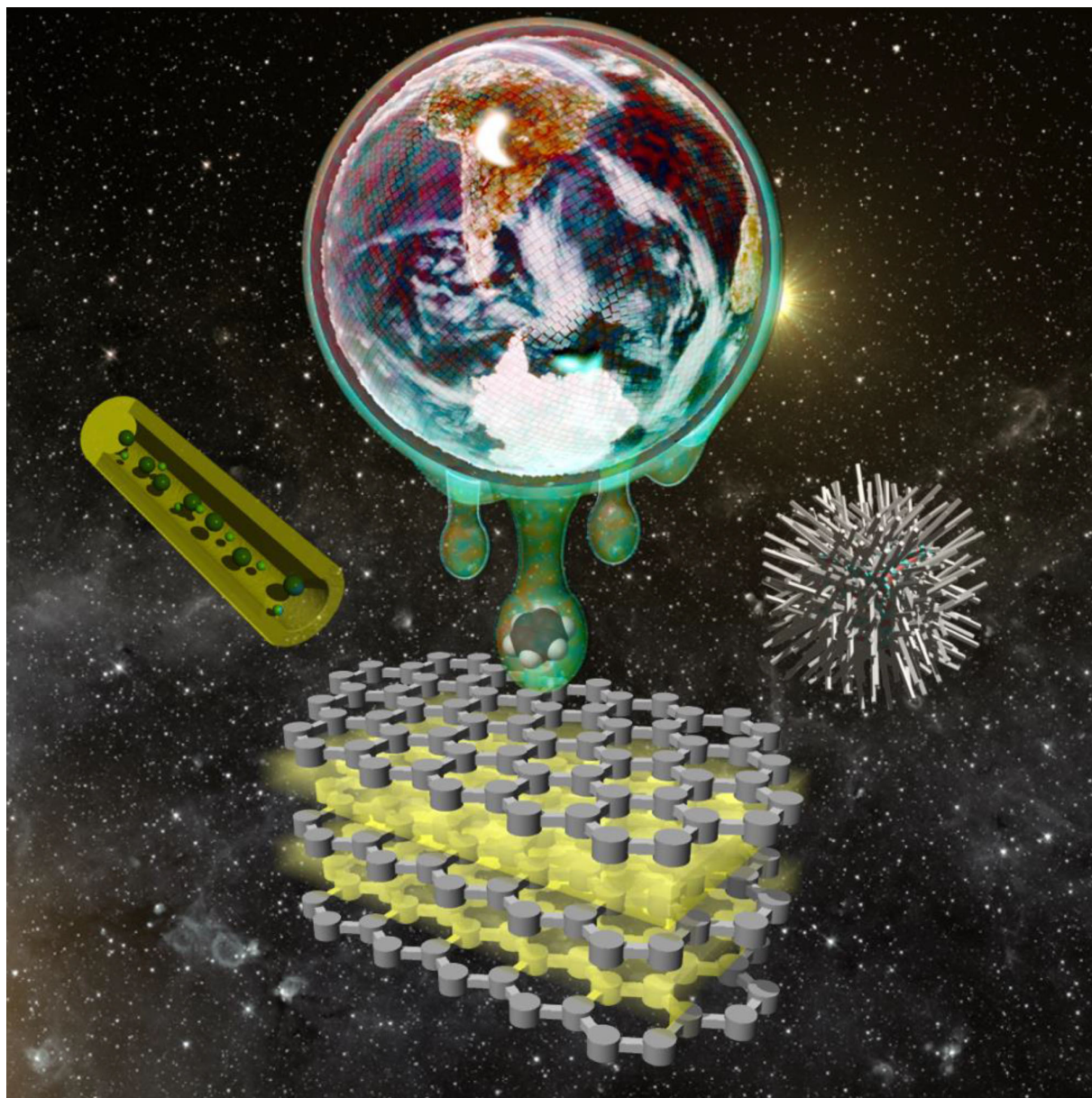


Nanoarchitectonic-Based Material Platforms for Environmental and Bioprocessing Applications

Katsuhiko Ariga,^{*,[a, b]} Joshua A. Jackman,^[c, d] Nam-Joon Cho,^{*,[c, e]} Shan-hui Hsu,^[f]
Lok Kumar Shrestha,^[a] Taizo Mori,^[a, b] and Jun Takeya^[b]



Abstract: The challenges of pollution, environmental science, and energy consumption have become global issues of broad societal importance. In order to address these challenges, novel functional systems and advanced materials are needed to achieve high efficiency, low emission, and environmentally friendly performance. A promising approach involves nanostructure-level controls of functional material design through a novel concept, nanoarchitectonics. In this account article, we summarize nanoarchitectonic approaches to create nanoscale platform structures that are potentially useful for environmentally green and bioprocessing applications. The introduced platforms are roughly classified into (i) membrane platforms and (ii) nanostructured platforms. The examples are discussed together with the relevant chemical processes, environmental sensing, bio-related interaction analyses, materials for environmental remediation, non-precious metal catalysis, and facile separation for biomedical uses.

Keywords: bio-process, catalysis, interface, nanoarchitectonics, sensing

1. Introduction

Human efforts have continuously promoted the development of advanced science and technology possibilities ranging from theoretical insights to innovative applications, including device technologies,^[1] molecular transformations,^[2] energy and signal conversions,^[3] materials production,^[4] and biological/biomedical inventions.^[5] The impact of science and technology continues to evolve, and there is growing attention to nanoscience and nanotechnology – the study and application of nanostructured materials that exhibit unique properties compared to their bulk counterparts. At the same time, one negative consequence of these technological developments is the growing impact of issues such as pollution, environmental damage, and energy consumption, which have shifted from local matters to global challenges of highest priority. In order to solve these problems, functional systems and materials are needed to achieve high efficiency,

low emission, and environmentally friendly performance while providing value-added innovations.^[6] Such capabilities will be partially accomplished through the innovation of functional materials with sophisticated organic synthesis,^[7] advanced materials fabrication,^[8] supramolecular organization,^[9] and bio-related processes^[10] along with more rigorous application of theoretical and experimental insights.^[11] In addition to the creation of innovative material composition, achieving control over their structural properties is of paramount importance. One particularly important aspect is precise control of functional structures in systems and materials. As such, scientific research efforts on materials of incredibly small size can lead impactful solutions to global problems.^[12]

Nanotechnology encompasses a unifying scientific and technological framework for fabricating ultra-small objects,^[13] which had led to tremendous accomplishments through observation, analysis, fabrication, and functionalization at the atomic and molecular scales with nanometer dimensions. The knowledge and skills obtained through nanotechnology can be integrated into the construction of functional systems and materials with nanoscale units through fusion with the other scientific and technological disciplines, supramolecular chemistry^[14] and related bottom-up nanofabrication approaches.^[15] The interdisciplinary fusion of these fields has created a novel scientific concept, nanoarchitectonics (Figure 1).^[16]

This emerging concept, nanoarchitectonics, originated by Prof. Masakazu Aono who first used the nanoarchitectonics term in the conference title of the 1st International Symposium on Nanoarchitectonics Using Suprainteractions in 2000.^[17] Based on this concept, functional material systems can be constructed from atoms, molecules, and nanoscale units through atom/molecular-level manipulations, modification of unit molecules with chemical procedures, fabrication of nano/microstructures by physical methods, supramolecular self-assembly/self-organization, and structural rearrangement by external stimuli and forces.^[18] The design strategy in

[a] Prof. Dr. K. Ariga, Dr. L. K. Shrestha, Dr. T. Mori
WPI Research Center for Materials Nanoarchitectonics (MANA),
National Institute for Materials Science (NIMS), 1–1 Namiki,
Tsukuba, Ibaraki 305-0044, Japan

E-mail: ARIGA.Katsuhiko@nims.go.jp

[b] Prof. Dr. K. Ariga, Dr. T. Mori, Prof. Dr. J. Takeya
Graduate School of Frontier Sciences, The University of Tokyo
5-1-5 Kashiwanoha, Kashiwa, Chiba 277-8561, Japan

[c] Dr. J. A. Jackman, Prof. Dr. N.-J. Cho
School of Materials Science and Engineering, Nanyang Technological University
Singapore, 637553, Singapore

[d] Dr. J. A. Jackman
Department of Medicine, Stanford University
Stanford, California, 94305, USA

[e] Prof. Dr. N.-J. Cho
School of Chemical and Biomedical Engineering, Nanyang Technological University
Singapore, 637459, Singapore

[f] Prof. Dr. S.-h. Hsu
Institute of Polymer Science and Engineering, National Taiwan University, No. 1, Sec. 4 Roosevelt Road, Taipei 10617, Taiwan, R.O.C.

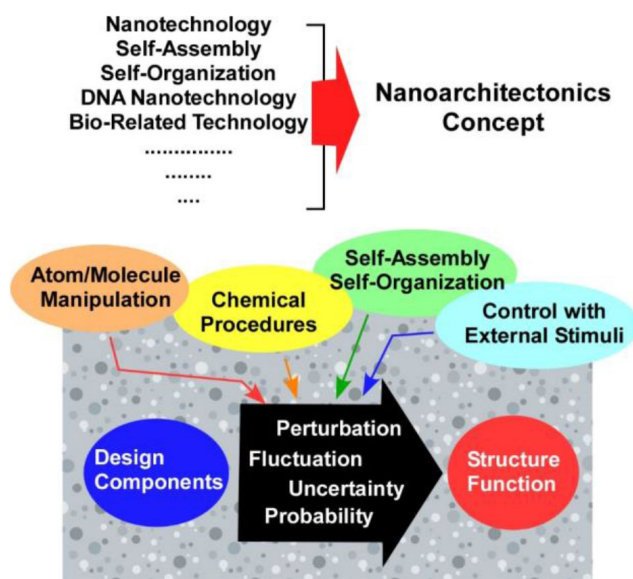


Figure 1. Outline of nanoarchitectonics concept, where harmonization of molecular-level interactions and dynamic processes arising from various interactions are crucial.

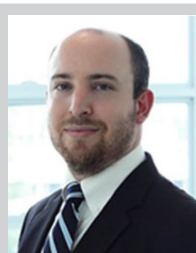
nanoarchitectonics is rather distinct from those observed in microscopic and macroscopic architectonics. While fabricated structures at the microscopic and macroscopic scales are based on exact construction blueprints (structural designs) between the various components, nanoarchitectonics are influenced, often in unpredictable ways, by numerous factors such as statistical distributions and thermal fluctuations. In nanoarchitectonic processes, the harmonization of molecular-level

interactions and dynamic processes arising from these interactions are emphasized.^[19] Due to the universal nature of the nanoarchitectonics concept, it can be applied to various research fields, including nanostructure regulation,^[20] nano-related fabrication of devices,^[21] nanomaterial production,^[22] catalysis,^[23] sensing,^[24] energy and environmental sciences,^[25] and biological and biomedical applications.^[26] Some examples of nanoarchitectonics suggest its potential for spurring innovations in green chemistry and green syntheses.^[27]

In this account article, we summarize nanoarchitectonic approaches to fabricate platform structures that are potentially useful for environmentally green and bioprocessing applications, as reported by our group and collaborators. These examples are explained together with their relevant chemical processes, environmental sensing, bio-related interaction analyses, materials for environmental remediation, non-precious metal catalysts, and facile separation for biomedical uses. The introduced platforms are roughly classified into (i) membrane platforms and (ii) nanostructured platforms, while nanoarchitectonic strategies are purposefully devised across these platform concepts. In the perspective part, we propose a novel concept for describing interfacial (or Langmuir) nanoarchitectonics^[28] as an innovative methodology to achieve energy-efficient control over molecular systems, including molecular machines.

2. Membrane Platforms

Thin films and membranes on surfaces are attractive sensing platforms that enable the conversion of material responses into device signals. Therefore, forming biomimetic platforms on device interfaces such as electrode and transistor surfaces is



Joshua A. Jackman is a Postdoctoral Fellow in the Stanford University School of Medicine. He received his Ph.D. in Materials Science and Engineering from Nanyang Technological University in Singapore. His research interests are focused on the development of acoustic and optical sensors for biointerfacial science and translational medicine applications.



Nam-Joon Cho is an Associate Professor in the School of Materials Science and Engineering at Nanyang Technological University. He leads the Engineering in Translational Science group, which focuses on applying engineering strategies to solve medical problems. His team's research



activities include biosensing tools, biomaterials, drug delivery, and anti-infective drug development.

Katsuhiko Ariga received his Ph.D. from Tokyo Institute of Technology in 1990. He is currently the Leader of the Super-molecules Group and Principal Investigator at the World Premier International Research Centre for Materials Nanoarchitectonics, NIMS. He has also been appointed as Professor at the University of Tokyo.

a promising way to fabricate environmental monitoring systems.

2.1. Layer-by-Layer Assembly: Sensing

Among various techniques for fabricating membranes such as the self-assembled monolayer method,^[29] Langmuir-Blodgett (LB) technique,^[30] layer-by-layer (LbL) assembly,^[31] and various vapor-phase deposition methods,^[32] the LbL assembly approach has key advantages in terms of the materials that can be used, including polymers, inorganic substances, quantum materials, nanocarbons, supramolecular assemblies, and biomaterials, as well as easy and versatile technical procedures. In the following sections, our approaches to fabricate membrane platforms based on LbL assemblies for environmental sensing, sustainable drug release, and bio- and electrochemical catalysis applications are introduced.

Nanoarchitectonic unit materials with specific shapes and electronic properties in layer-by-layer structural motifs would provide nanopspaces that are advantageous for sensing applications.^[33] For example, two-dimensional materials such as graphene, graphene oxides, and MoS₂ have perfectly extended flat structures with unique electronic and electrochemical properties.^[34] Interlayer spaces between the assembled two-dimensional unit materials would become two-dimensional nanopspaces appropriate for accommodating and detecting molecules with particular sizes, shapes, and electronic properties. In order to prepare unit materials for layer-by-layer assemblies composed of graphene and ionic liquid (Figure 2),^[35] graphene oxide nanosheets were prepared by the oxidization of graphite under acidic conditions and the

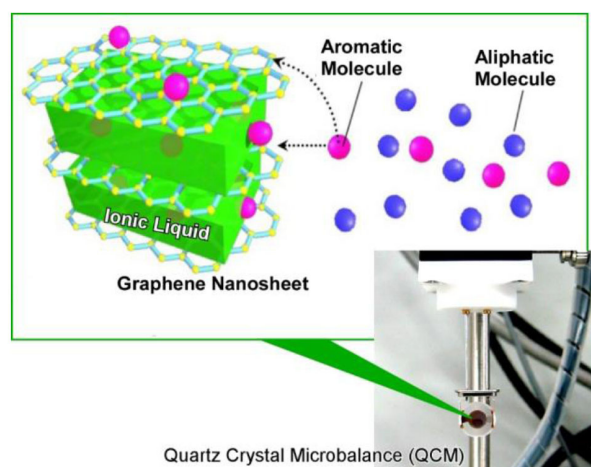


Figure 2. Layer-by-layer assemblies of graphene and ionic liquid layers on a QCM sensor for toxic (aromatic) gas sensing.

reduction of graphene nanosheets was carried out in the presence of ionic liquids under aqueous conditions. The resulting alternating layer structures of reduced graphene oxide and aromatic liquids were further assembled with poly (sodium styrenesulfonate) (PSS) by the LbL method on the surface of a quartz crystal microbalance (QCM) sensor. The composed sensors were subjected to environmental monitoring for the detection of various organic gas molecules. The sensor exhibited higher selectivity for benzene vapor over cyclohexane although they have similar molecular sizes, molecular weights, and vapor pressures. Aromatic ionic liquid interlayer nanopspaces between graphene nanosheets provide π -electron-rich environments for selective detection of aromatic gas guest molecules. In addition, enhanced detection toward CO₂ gas from a saturated sodium hydrocarbonate solution to layer-by-layer films of reduced graphene oxide and aromatic ionic liquid was also confirmed.

The high-surface area of nanostructured materials would be an advantageous feature for sensing applications. Various materials with high surface area and large pore volume such as mesoporous materials,^[36] nanoporous structures,^[37] and metal organic frameworks (coordination polymers)^[38] are good candidates as sensing materials with superior sensitivity. For the fabrication of layer-by-layer structures composed of mesoporous carbon and polyelectrolytes, surface-oxidized mesoporous carbon (CMK-3) with negative charge was assembled alternately with positive polyelectrolytes such as poly (diallyldimethylammonium chloride) into layered structures on a QCM plate.^[39] The performance of the fabricated QCM sensors was investigated under aqueous conditions though the injection of target molecules to the test aqueous solution. Detection of tannic acid by measuring frequency shifts of the QCM sensors was more sensitive than for other tested samples, including catechin and caffeine. The observed high affinity to tannic acid likely originates from enhanced π - π interactions and hydrophobic effect upon size matching between guest molecules and nanopore channels. In addition, the highly cooperative nature underpinning the adsorption of tannic acid molecules onto mesoporous carbon LbL films exhibited a sigmoidal adsorption profile at low guest molecule concentrations. This cooperativity is likely due to enhanced guest-guest interactions within the confined carbon nanopspaces.

As high surface-area materials with hierarchical structures, mesoporous carbon capsules as sensing unit materials were assembled in a layer-by-layer manner together with polyelectrolytes on QCM sensor electrodes (Figure 3).^[40] The mesoporous carbon capsules (1000 × 700 × 300 nm³ dimensions) possessed a homogeneous 35-nm thick carbon shell that has a mesoporous structure with a uniform pore size distribution centered at 4.3 nm in diameter and a specific surface area of 918 m² g⁻¹. The fabricated QCM sensor with

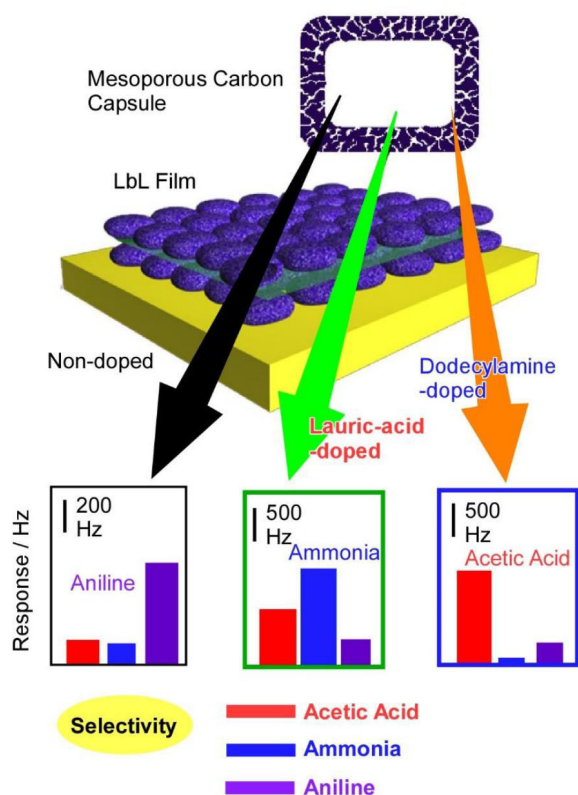


Figure 3. Layer-by-layer films of mesoporous carbon capsules with polyelectrolyte on a QCM sensor electrode whereby selectivity can be altered through impregnation of the second recognition component within the capsule structure.

the mesoporous carbon capsule in LbL film architecture showed high sensitivity to aromatic organic compounds in the gas phase along with expected selectivity. However, this selectivity can be altered through impregnation of the second type of recognition component within the capsule structure. Doping with the carboxylic acid functional group of lauric acid resulted in shifts of the detection selectivity to aliphatic amines, while increased affinity to acetic acid was attained by impregnation with dodecyl amines. The observed tunability of guest selection along with structural stability of carbon materials is advantageous for the fabrication of sensors and separation membranes with desirable selectivity. In a similar sensing system, pre-coating of mesoporous carbon capsules with polyelectrolytes and surfactants also alters sensing selectivity.^[41] For example, coating with poly(styrene sulfonate) increases accessibility to vapors of aromatic gas molecules due to the aromatic nature of poly(styrene sulfonate), resulting in enhanced selectivity to aromatic guest molecules. By contrast, coating with poly(allylamine

hydrochloride) lowers the accessibility of guest vapors due to partial blocking of the pores.

2.2. Layer-by-Layer Assembly: Release and Delivery

Advancing similar nanoarchitectonic principles, layer-by-layer films of mesoporous silica capsules with interior volumes of $1000 \times 700 \times 300 \text{ nm}^3$ and a mesoporous silica wall with average diameter of 2.2 nm are capable of the automatic stepwise release of water and liquid-phase drug molecules from the interior reservoir to external environment.^[42] The films were prepared by LbL assembly between anionic mesoporous silica capsules and cationic polyelectrolyte materials with the aid of anionic silica nanoparticles on a QCM plate for quantitative monitoring of material release behaviors. Release profiles of water from the capsule films to the air phase exhibited auto-regulated step-wise behaviors, i.e., spontaneous release and stop sequences without any external stimuli. Similar phenomena were observed in the release process of liquid drug molecules from the capsule films to the air phase. Liquid substance entrapped in the mesoporous channels of the external silica walls initially evaporated and the rate slowed down with a continuous decrease in the release rate. Liquid evaporation eventually stopped, and then the liquid was supplied from the interior reservoir to external mesoporous channels upon exchange with air molecules. These processes result in the alternate sequence of release and stop without requiring external controls. This is an interesting, yet counterintuitive example because all other types of controlled release need input from one or more external stimuli. Hence, the approach can be regarded as a green energy-free process of material release and transfer.

Layer-by-layer films prepared from DNA oligonucleotide-modified MoS_2 nanosheets through the formation of superstructures guided by a linker aptamer that can be used for drug encapsulation and ATP-driven drug release.^[43] Drugs incorporated within the interlayer spaces of MoS_2 nanosheets can be protected from external disturbances. However, ATP diffusion into the interlayer nanospace causes disassembly of the layer-by-layer structure upon stronger binding of ATP to the linker aptamer, resulting in release of entrapped drug molecules. According to this nanoarchitectonic design strategy, the release of drug molecules, the doxorubicin anticancer drug in this case, can be induced through the disassembly of the layer-by-layer structures in the presence of the highly metabolically active environment of cancer cells.

2.3. Layer-by-Layer Assembly: Green Reactions and Catalysis

Nanoarchitectonic structures based on LbL assembly can be applied to green catalytic processes including bioreactors. Because the LbL assembly process can be done under mild conditions, the incorporation of active biomolecules such as enzymes is a promising nanoarchitectonic output.^[44] The flexibility in film-layering sequences is also advantageous to fabricate multi-enzyme reactors with orchestrated reaction sequences. For example, an efficiency-optimized reactor to go from starch to gluconolactone via glucose designed by organizing an upper layer of glucoamylase (for conversion of starch to glucose) and a bottom layer of glucose oxidase (from glucose to gluconolactone) on an ultrafilter reactor (Figure 4).^[45] Passing a starch solution through the ultrafilter with two kinds of enzymes successfully converted starch to glucose and gluconolactone with separation of excess starch.

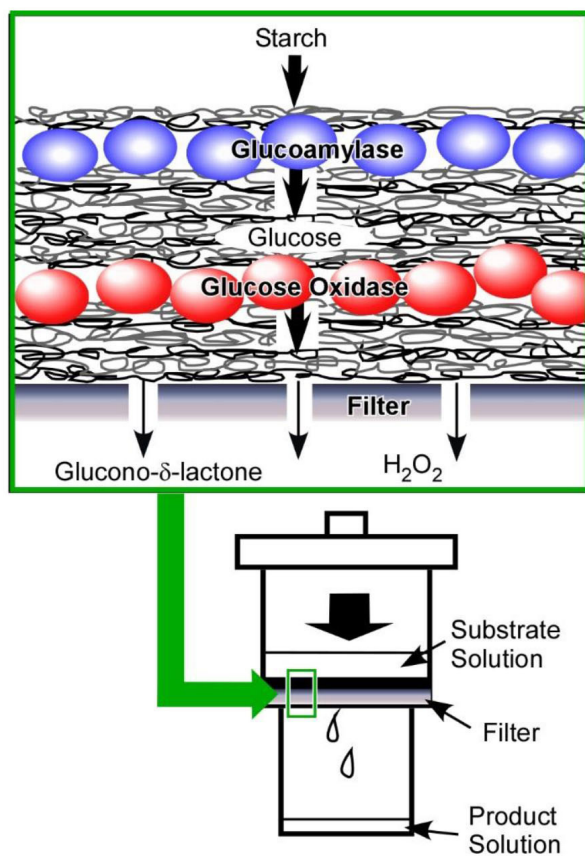


Figure 4. Layer-by-layer enzyme reactor from starch to gluconolactone via glucose with upper layer of glucoamylase (for conversion of starch to glucose) and bottom layer of glucose oxidase (from glucose to gluconolactone) on ultrafilter reactor.

In this case, the incorporation of polyelectrolyte layers in between glucoamylase and glucose oxidase layers is crucial to avoid interference between the activities of the two enzymes. Another advantage of the enzyme reactor involving the LbL assembly coating is greatly enhanced stabilities of the enzymes with respect to temperature, solution pH, and performance duration.^[46] In addition, the LbL film structures have imperfect packing, as compared to Langmuir-Blodgett (LB) films, and this format is advantageous for substrate permeation.^[47]

For green catalysts, metal-based LbL film structures have also been explored. For example, all-metallic layer-by-layer films with mesopores Pt/Pd bimetallic structures were prepared with the assistance of micelle self-assembly in a dilute surfactant electrolyte.^[48] The nanoarchitected bimetallic layer-by-layer films exhibited enhanced electrocatalytic activity for methanol oxidation. The mesoporous nature of the architected films is advantageous for supplying a large surface area to the active sites and suppressing undesirable agglomeration of catalytic species. Indeed, the mesoporous metallic films showed greater electrocatalytic activities for a long duration as compared to commercial Pt black catalysts. The bimetallic Pt/Pd layer-by-layer film exhibited higher electrocatalytic activity than even monometallic mesoporous Pt materials. Formation of atomic-level Pt-to-Pd contacts was achieved without any voids or holes at the interlayer interface between Pt and Pd layers, resulting in a Pt/Pd alloy nanoarchitecture. The latter structure is capable of promoting cleavage of C–H bonds as part of methanol decomposition. Further optimization of the metallic components and layer sequences could potentially lead to the development of sensors, reactors, and catalysts for green purposes.

The highly popular materials, graphene oxide and coordination polymers, were assembled in a layer-by-layer structure as highly durable catalysts for the oxygen reduction reaction.^[49] These layer-by-layer structures were fabricated through the deposition of Ni-based cyanide-bridged coordination polymer flakes on the surfaces of graphene oxide nanosheets, where the graphene oxide nanosheets worked as nucleation sites to promote crystal growth of Ni-based cyanide-bridged coordination polymers. The fabricated layer-by-layer films showed outstanding electrocatalytic activity for the oxygen reduction reaction and exhibited excellent durability.

2.4. Supported Lipid Bilayer: Formation Analysis

Supported lipid bilayers (SLBs) would be one of the most promising biomimetic platforms to study green processes at biomembrane interface. The nanoarchitectonics of SLB formation and interactions with external materials such as vesicles, peptides, and viruses have been extensively inves-

tigated. Indeed, SLBs are an important model membrane platform that are widely utilized in biosensing, surface functionalization, and cellular interface applications.^[50] The earliest work in the field originated by studying vesicle adsorption onto solid supports. On silicon dioxide surfaces, adsorbed vesicles typically rupture to form a two-dimensional SLB, while adsorbed vesicles remain intact on gold and titanium oxide surfaces.^[51] These different self-assembly pathways were first identified by employing quartz crystal microbalance with dissipation monitoring (QCM-D) measurements, which are sensitive to the mass and viscoelastic properties of adsorbed phospholipid molecules, and set a high measurement standard for biological surface science applications.^[52] Such capabilities can distinguish adsorbed vesicles, which possess a large fraction of hydrodynamically-coupled solvent, from an SLB that has a low fraction of hydrodynamically-coupled solvent. In recent years, there has been growing interest to develop methods to fabricate SLBs on historically intractable surfaces, and QCM-D measurements have helped identify that solution pH can be adjusted to modulate the vesicle-substrate interaction strength.^[53] In particular, by controlling the vesicle-substrate interaction strength, it was shown that acidic conditions promoted vesicle adsorption and spontaneous rupture to form an SLB on titanium oxide surfaces, while alkaline conditions inhibited the rupture of adsorbed on silicon dioxide surfaces.

It has also been possible to identify that the direction and magnitude of the osmotic pressure across a vesicle's lipid bilayer can either promote or inhibit the rupture of adsorbed vesicles on silicon dioxide surfaces.^[54] Positive osmotic pressures induced vesicle rupture to form SLBs, and negative osmotic pressures inhibited rupture of adsorbed vesicles and hence prevented SLB formation. Another key parameter is the quality of the vesicle preparation, and it has been shown that freeze-thaw pretreatment of vesicles increases unilamellarity and hence improves SLB quality.^[55] QCM-D measurements revealed that using untreated vesicles to fabricate SLBs led to a higher number of defects indicative of unruptured vesicles. More recently, it was demonstrated that, by systematically varying solution pH and membrane surface charge, it is possible to control vesicle adsorption behavior on silicon dioxide surfaces.^[56] Five different pathways were identified, including (i) complete SLB formation, (ii) incomplete SLB formation, (iii) irreversible vesicle adsorption, (iv) reversible vesicle adsorption, or (v) no adsorption, and the experimental results were consistent with the corresponding trend in vesicle-substrate interaction strength (Figure 5). In the aforementioned examples, QCM-D measurements provided the key characterization tool to characterize vesicle adsorption kinetics and enabled a deep understanding of how surface-specific adsorption behaviors can be modulated by varying

environmental conditions in a rational manner that either strengthens or weakens the vesicle-substrate interaction.

In another direction, novel strategies to form SLBs have been explored that bypass the relatively high energetic requirements needed to rupture adsorbed vesicles^[57] and take advantage of how phospholipid molecules self-assemble into different phases depending on the solvent system.^[58] Based on this approach, a particularly interesting strategy was developed that is called the solvent-assisted lipid bilayer (SALB) method and involves phospholipid deposition in a water-miscible organic solvent before a solvent-exchange step is performed to replace the bulk organic solution with aqueous solution.^[59] The latter step induces SLB formation and the entire fabrication process can be quickly performed and does not require vesicle preparation. Importantly, the SALB method enables bilayer formation on not only silicon dioxide surfaces but also formerly intractable surfaces such as gold and titanium oxide. QCM-D measurements have been employed to monitor SLB formation kinetics, including defining main requirements such as the solvent-exchange flow rate and the bulk lipid concentration.^[60] The importance of these governing parameters was further confirmed by additional experimental techniques, simulations, and theoretical analysis,^[61] highlighting the utility of QCM-D measurements for detailed characterization efforts and leading to establishment of an optimized SALB protocol (Figure 6).^[62] It was further identified that the SALB method can form SLBs on aluminum oxide,^[63] and the high sensitivity of the QCM-D technique to hydrodynamically-coupled solvent led to the identification of a particularly thick hydration layer separating SLBs from the underlying aluminum oxide surface. The SALB method has also been demonstrated to fabricate SLBs containing high cholesterol fractions for the first time^[64] (up to ~63 mol % cholesterol; other methods are limited to ~20 mol % cholesterol^[65]), and the QCM-D technique facilitated quantitative determination of the cholesterol fraction in the SLB by methyl- β -cyclodextrin treatment.

The use of bicellar disks to form SLBs has also gained attention as a promising fabrication method that does not require vesicle preparation.^[66] Bicellar disks are composed of a mixture of long-chain and short-chain phospholipids, and QCM-D measurements have proven to be an important characterization tool for optimizing SLB formation, including defining appropriate molar ratios of the two phospholipids.^[67] Of note, QCM-D measurements identified that optimal SLB formation occurs at relatively low total phospholipid concentrations in order to minimize the detergent-like effects of short-chain phospholipids and hence obtain high-quality SLBs.^[68] Taken together, the QCM-D technique has proven to be a broadly useful measurement approach to characterize conventional SLB fabrication approaches as well as to support the development of new fabrication approaches.

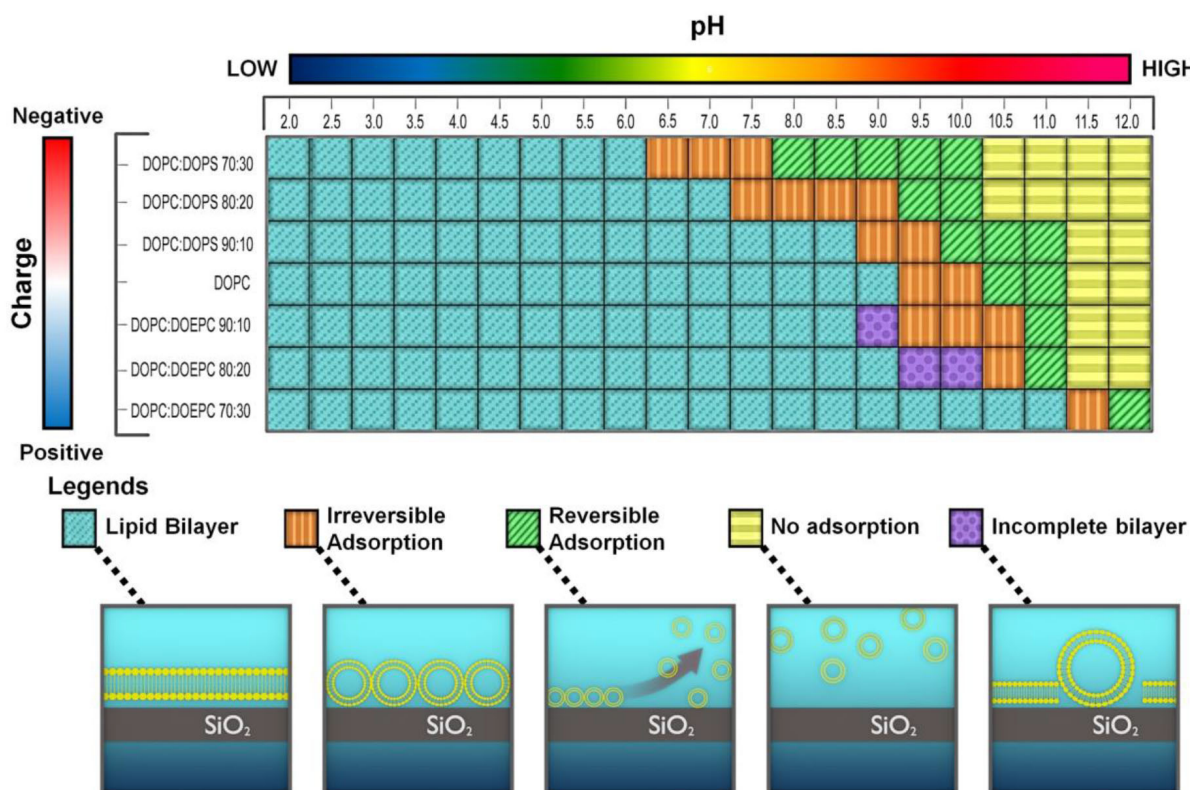


Figure 5. QCM–D measurement profiling of vesicle adsorption onto a silicon dioxide surface. Experiments were conducted as a function of solution pH and membrane surface charge (by varying the lipid composition). DOPC, DOPS, and DOEPC are neutral, anionic, and cationic phospholipids, respectively. The color scheme in each box corresponds to the measured morphological properties of the resulting lipid adlayer. Reprinted with permission from Ref. [56]. Copyright 2018 American Chemical Society.

2.5. Supported Lipid Bilayer: Interaction Analysis

While the QCM–D technique is often recognized as a powerful tool to track SLB formation kinetics, it has also demonstrated excellent utility for monitoring vesicle adsorption in cases where the adsorbed vesicles remain intact. Typically, the QCM–D technique is employed to characterize the properties of adsorbed vesicle layers at saturation coverage.^[69] For example, QCM–D experiments provided supporting evidence to implicate a strong hydration force as the key factor preventing the rupture of adsorbed vesicles on titanium oxide.^[70] However, one general challenge of the QCM–D technique is that the measurement signals are not proportional to the surface coverage of adsorbed vesicles.^[69a] The nonlinear responses occur due to the motion of adsorbed vesicles and hydrodynamically-coupled solvent along with lateral interactions between adsorbed vesicles.^[69,71] As such, conventional QCM–D models are generally limited to saturation coverage and treat the adsorbed vesicle layer as a

homogenous film.^[72] Motivated by these factors, there has been strong interest in developing QCM–D measurement approaches to characterize adsorbed vesicles at low surface coverages where there is negligible hydrodynamic coupling.

To address this outstanding need, a QCM–D model was recently developed based on hydrodynamic simulations in order to extract the size of adsorbed, spherical particles at low surface coverages.^[73] The measurement analysis enabled accurate size characterization of adsorbed vesicles under conditions where adhesion-induced vesicle deformation was negligible. The model was further refined in order to characterize the deformation of non-spherical, adsorbed vesicles as well.^[74] The model was applied to QCM–D measurement data pertaining to the adsorption of fluid-phase and gel-phase vesicles onto a titanium oxide surface under different osmotic pressure conditions. By determining which osmotic pressure condition induced the onset of vesicle deformation, it was possible to determine the membrane bending energy of adsorbed vesicles and the results agreed

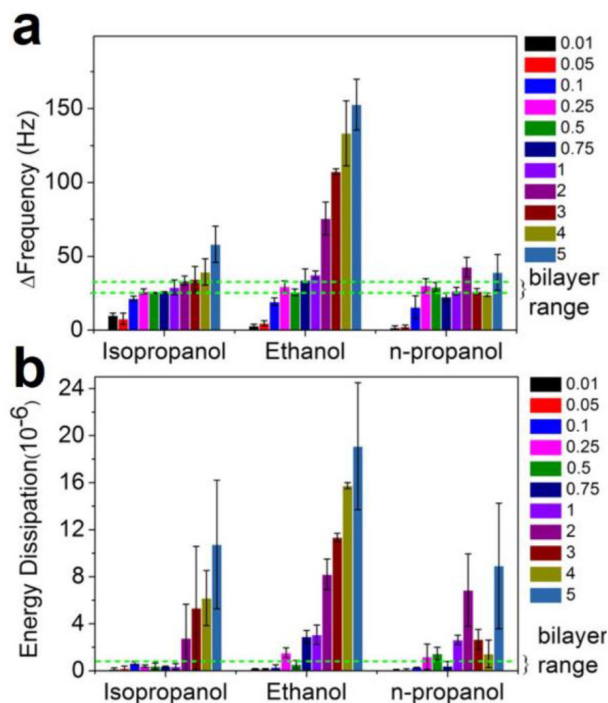


Figure 6. Effect of bulk lipid concentration on supported lipid bilayer formation by the SALB method. QCM–D experiments were conducted using different organic solvents, including isopropanol, ethanol, and n-propanol. The final QCM–D responses are reported for the a) frequency and b) energy dissipation shifts. The dashed lines correspond to the range of frequency and dissipation shifts that are typical for a complete bilayer. Reprinted with permission from Ref. [60]. Copyright 2015 American Chemical Society.

with literature values (Figure 7). The measurement approach was further utilized to understand how glucose affects vesicle-membrane interactions by increasing the intermembrane contact area while not affecting the height of adsorbed vesicles.^[75] Specifically, it was reasoned that there is depletion of glucose molecules from the intermembrane hydration layer, which increases the corresponding adhesion force. The collective body of work highlights how the QCM–D technique can be utilized to quantitatively measure the size and deformation of adsorbed particles at low surface coverage.

To increase applicability, the model was extended to analyze QCM–D measurement data across different surface coverage regimes, including intermediate surface coverages.^[76] This broader range was achieved by conducting lattice Boltzmann simulations of adsorbed rigid particles attached to an oscillating surface. The simulation results provided insight into how fundamental parameters such as particle size and interparticle distance affect QCM–D measurement responses, and the trends agreed with experimental data. The findings

also provided a theoretical basis for a previously reported empirical method to extract the size of adsorbed particles at high surface coverage.^[77] Altogether, the demonstrated measurement capabilities support that developing phenomenological models based on hydrodynamic simulations is a promising strategy to improve QCM–D measurement analysis.

3. Nanomaterial Platform

As mentioned above, membrane-based platforms are highly suitable for nanoarchitectonics for green-related functions such as environmental sensing, bio-interactions and environmentally friendly, high-performance catalysts. In addition to membrane-type forms, additional nanomaterial designs incorporating nanoarchitectonic principles have been applied to design various nanostructured systems. In the following sections, various nanomaterial platforms are introduced according to purpose-oriented classifications.

3.1. Environmental Risk Detection: Nanoporous Materials

For the exploration of environmentally friendly materials synthesis and system design options, evaluating measurement capabilities to detect environmental risks such as toxic substances is a necessary step. Nanomaterials with integrated structures often provide appropriate platforms for sensing due to promoting contact between sensing materials and target substances. Well-designed nanoporous and mesoporous materials are capable of detecting external substances on the basis of their high-surface-area properties and facile molecular diffusion within the nanostructures.^[78] For example, nanoporous carbon materials prepared by direct carbonization of Al-based porous coordination polymers were immobilized on a QCM sensor with the aid of polyelectrolyte binders.^[79] The fabricated QCM sensor exhibited high detection selectivity to toxic aromatic gas substances as indicated by three-times greater sensitivity to benzene over cyclohexane and hexane. The enhanced sensitivity to aromatic gas substances is likely due to π – π interactions between aromatic guest molecules and the graphitic carbon framework.

A beneficial advantage of mesoporous materials in nanoarchitectonics is the wide range of possibilities for nanostructure design and component selection. Nitrogen-incorporated mesoporous carbon can be synthesized from a low-cost green material source, gelatin, through nanocasting methods with mesoporous silica, SBA-15, as a hard template.^[80] The fabricated mesoporous materials have a highly basic nature based on which highly selective sensing of acetic acid was demonstrated. Similarly, graphitic mesoporous carbon nitride was successfully prepared by polymerization of 3-amino-

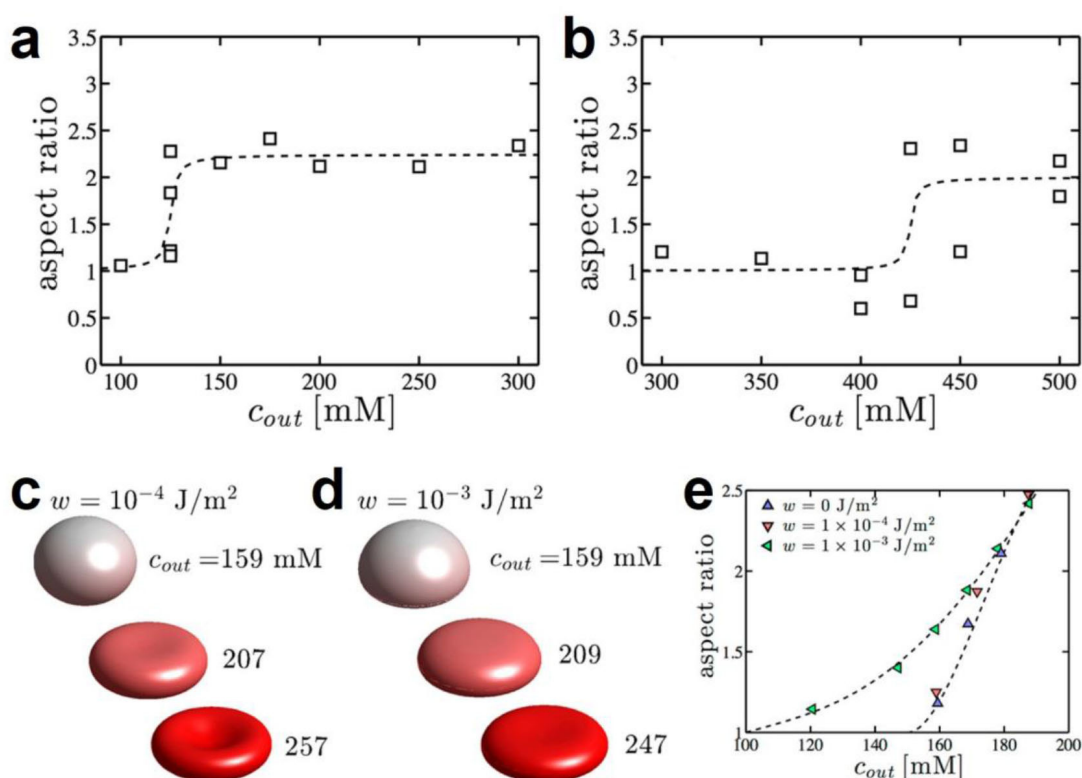


Figure 7. Experimentally measured aspect ratio as a function of external ionic strength (c_{out}) for a) fluid-phase DOPC and b) gel-phase DPPC lipid vesicles. Each data point represents an independent experiment. c,d) Theoretical shapes of fluid-phase lipid vesicles as a function of external ionic strength (c_{out}) for a relatively c) small or d) large surface adhesion energy (w), respectively. e) Theoretical aspect ratio as a function of external ionic strength (c_{out}) for various surface adhesion energies (w) for fluid-phase lipid vesicles. Reprinted with permission from Ref. [74]. Copyright 2018 American Chemical Society.

1,2,4-triazine within nano-channels of a hard template.^[81] The fabricated materials have basic carbon nitride frameworks that are advantageous for sensing acidic substances. In this case, formic acid was sensitively detected. Immobilization of enzymes onto porous materials enables the fabrication of biosensors. Porous carbon films with immobilized glucose oxidase was reported to be an excellent platform for glucose sensing.^[82] Sensitivities can be tuned by the amount of glucose oxidase as well as the pore diameter. The fabricated biosensor exhibited high stability and high reproducibility.

To achieve green synthesis of functional nanoporous materials, nanoporous carbon materials were prepared through phosphoric acid activation of low-cost agro-waste corncob powders.^[83] The synthesized nanoporous carbon materials showed rather good maximum specific capacitance with stable capacitance retention even after 1000 cycles. Moreover, the nanoporous carbon materials were suitable nanomaterial platforms of sensing applications. Unlike other nanoporous carbon materials, the corncob-powder-derived nanocarbons exhibited higher sensitivities to formaldehyde,

acetic acid, and ammonia detection, as compared to aromatic carbon gasses. Of note, particularly large sensitivity to ammonia was observed, which could be due to the presence of carboxylic acid groups on the nanomaterial surface.

Similarly, nanoporous carbon materials were also prepared from another naturally abundant biomaterial, bamboo, through chemical activation with phosphoric acid at 400 °C.^[84] Fourier transform-infrared (FT-IR) spectroscopic analyses indicated the presence of various functional groups such as carboxylate, carbonyl and phenolic groups at the surface of the carbon materials. These functional groups are important because they facilitate interactions with guest molecules possessing hydrogen-bonding groups. Therefore, sensing selectivity to various gas substances was observed in the order of acetic acid (highest), methanol, ethanol, propanol, butanol, ethylbenzene, carbon tetrachloride, toluene, and benzene (lowest). Interestingly, this sensing system is capable of clearly discriminating C₁ and C₂ alcohols, i.e., methanol and ethanol. The latter capability represents an attractive sensing characteristic to distinguish between essen-

tial carbon sources for their separation and detection in fields such as the petroleum and food industries.

Based on the rational selection of template structures, pore-engineered mesoporous carbon materials can be designed according to nanoarchitectonic principles. One of the most successful examples is the so-called carbon nanocage, which can be synthesized through a hard-template nanocasting approach using cage-type mesoporous silica KIT-5.^[85] Carbon nanocages are useful structures for the sensitive separation of tea components and nucleic acid bases among other possibilities. For advanced sensing applications, carbon nanocage materials were immobilized on a QCM sensor plate with electrospun poly(methyl methacrylate) microfibers.^[86] The fabricated hierarchical cage-in-fiber architectures are advantageous for the sensitive detection of gaseous substances. In this case, the sensitivity for aniline is significantly higher than for a similar aromatic molecule, benzene, as indicated by distinct differences in their binding constants to the cage-in-fiber structures (1852.1 and 36.4 M⁻¹ for aniline and benzene, respectively). Carbon nanocage materials intrinsically support higher affinity to aromatic carbons through π - π interactions and the presence of a small amount of oxidized groups on the nanomaterial surface further promotes the detection of a basic aromatic molecule, aniline. Highly sensitive detection of aniline would be useful to diagnose lung cancer in the early stages by breath analysis alone.

Nanoporous structures can also be fabricated using biomaterials such as protein molecules. Though a soft-templating approach involving polystyrene spheres, cytochrome c protein molecules were assembled into a nanoporous-structured film.^[87] The prepared nanoporous protein films showed high performance stability as determined by long-duration electrochemical activity. Sensing performance to detect the vapors of gas molecules generally showed low affinities to organic vapors, including hexane, benzene, toluene, and cyclohexane. In marked contrast, sensitive detection of acidic gasses such as formic acid, acetic acid, and propionic acid was observed. Basic amino acid residues in cytochrome c molecules, which collectively form mesoporous structures, probably enabled the detection of acidic vapors. The highest sensitivity to the smallest tested molecule, formic acid, is consistent with the fact that smaller molecule diffuse more quickly within the nano-channels. Although simple acid-base interactions were utilized in this sensing system, more specific recognition capabilities can be accomplished by designing nanoporous protein films based on specific sequences of amino acids and/or protein secondary structures.

3.2. Environmental Risk Detection: Self-Assembled Structures

The fabrication of nanostructured platform is not limited to template synthesis as described above. Supramolecular processes arising from self-assembly and self-organization with possible post-treatment steps represent a promising methodology to create well-integrated and complex nanoarchitectures from rather simple unit molecules and materials through energy-efficient green procedures.^[88] For example, various types of nanoarchitectures can be fabricated from simple molecular units, such as fullerenes, by liquid-liquid interfacial precipitation.^[89] In this method, no energy supply or energy-consuming procedure is required. Well-structured nanoarchitectures can be spontaneously prepared by placing together two immiscible solutions. In some cases, the assembled structures can be converted into highly graphitic structures though energy-dependent high temperature processes, as seen in the synthesis and resulting sensor applications of π -electron-rich nanoporous carbon tubes from fullerene crystals.^[90] Simpler and energy-efficient post-treatment steps such as solvent washing are also possible to further process fullerene assemblies. Several examples describing the green fabrication of integrated nanoarchitectures from fullerene units are shown below.

Microscopic cubic-shaped assemblies of C₇₀ can be spontaneously fabricated upon liquid-liquid interface precipitation through gentle contact of a *tert*-butyl alcohol layer with C₇₀ mesitylene solution. Exposure of the fabricated microcubes to appropriate solvents induced partial dissolution of the cube surface and subsequent growth of nanorod antennas vertically from the cubic faces (Figure 8).^[91] In addition, every antenna nanorod possesses nanoporous material properties. Hierarchical micro/nano-architectures, namely antenna-on-cube C₇₀ assemblies, were prepared through specific sequences of solvent processes. Like insect antennas, the nanorods grown from central cubes enhanced sensing capabilities to detect gas molecules. A superior sensing capability for vapor-phase aromatic molecules was attained due to facile diffusion through the nanoporous architecture of the antenna, which promoted π - π interactions resulting in selective detection of toxic aromatic gas molecules.

Guest accommodation spaces are not limited to microscopic pores. Microscopic holes can also discriminate microscopic objects according to their surface characteristics. Hole-in-cube fullerene microscopic assemblies, in which one microscopic open-hole structure is located at the center of every face of C₇₀ microcubes, have been fabricated by liquid-liquid interfacial precipitation under dynamic conditions.^[92] The fabricated holes can be closed with the addition of extra C₇₀ molecules and re-opened by irradiation with electron beams. The open hole structure can discriminate between the

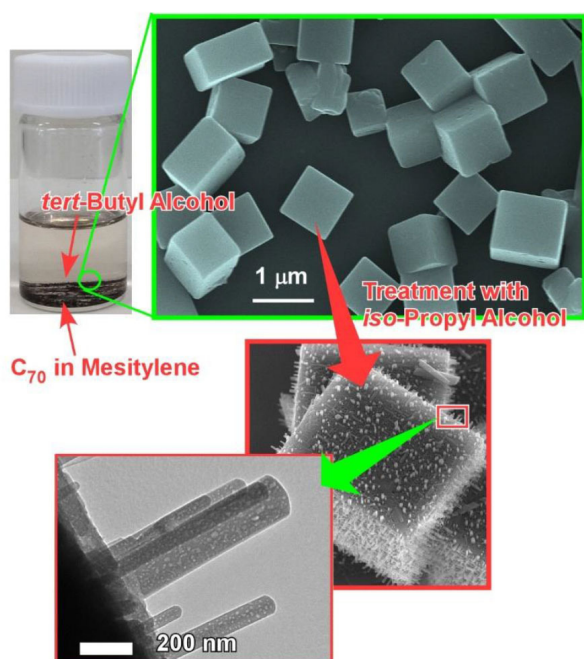


Figure 8. Microscopic cubic-shaped assemblies with growth of nanorod antenna vertically from the cubic faces as an antenna on the cube structure.

microspheres of graphitic carbon and conventional polymer resin. Preferential trapping of graphitic carbon spheres over polymer spheres was observed. The selection of spheres originated from preferential contact of the graphitic surfaces of microspheres with the sp^2 -rich carbon inner surfaces of C_{70} cubes. This microscopic recognition system is potentially useful for the detection and removal of toxic pollutant particles such as PM 2.5.

3.3. Environmental Risk Detection: Others

Recently, another class of sensitive sensor, termed the nano-mechanical membrane-type surface stress sensor, was developed for environmental gas sensing applications. Architecting nanostructures on membrane-type surface stress sensor plates often enhances sensitivity and modulates selectivity.^[93] Immobilizing silica flake-shell structures efficiently enhances the sensitivities of nanomechanical sensors while modification with tetraphenylporphyrin units can modulate selectivity.^[94] In this case, excellent performance with good measurement sensitivity and selectivity for acetone detection was achieved at low operating temperatures. This capability was significant because acetone detection is an important issue for the evaluation of metabolites in lipid metabolism and the

preservation of industrial environments. As such, the development of a portable, easy-to-use devices for monitoring local acetone levels can be accomplished through employing nano-architectonic designs of this kind to construct functional nanomaterials. In another embodiment, instead of using porphyrin units, hemoproteins were immobilized on the surface of silica flake shells in a membrane-type surface stress sensor configuration.^[95] In the latter case, high affinity for toxic H_2S gas molecules was confirmed, further demonstrating the potential to modulate sensing selectivity through surface modifications.

In light of the accident at the Fukushima Daiichi nuclear power plant, these nanoarchitectonic-based sensing platforms could potentially fill important needs to monitor the distribution of radioactive species, including ^{137}Cs , in the environment. In order to visually detect Cs ions in the environment, a novel reagent called Cesium Green has been developed.^[96] The presence of Cs ions in contaminated ground and within plant cells can be sensed by the bright fluorescence arising from the specific interaction between Cs ion and Cesium Green.^[97] In this case, part of the reagent's molecular probe binds to Cs ions while the there is a reporting part that emits fluorescent light. To develop a further improved system, the binding and reporting parts are assembled into the supramolecular assembly of an optode sensor (Figure 9).^[98] This system involves the assembly of a calix [6] arene derivative for Cs binding, proton supplier molecules, and proton-sensitive dyes in one film, thereby enabling the detection of Cs ions through colorimetric changes even in sea water and tap water. The presence of Cs ions in solution induced color changes of the films from yellow to blue, while the film color remain unchanged in the presence of solutions containing other environmentally abundant cations such as Na^+ , K^+ , Ca^{2+} , and Mg^{2+} . The system can be further configured into nanoparticles with a diameter of around 100 nm to realize nano-optode sensing possibilities. The latter system provides higher spatial resolution for measuring Cs ion distributions than existing radiosopes and gamma ray cameras.

3.4. Green Catalyst and Environmental Remediation: Nanostructure Control

Green catalysts for environmental remediation, green synthesis for catalysts with minimum environmental loads, and high-performance catalysts with abundant, cheap elements are important topics for realizing environmentally green processes.^[99] Not limited to the exploration of functional materials themselves, the well-considered design and fabrication of nanostructures often leads to incredible improvements in material performance as well. As such, material nanoarchitec-

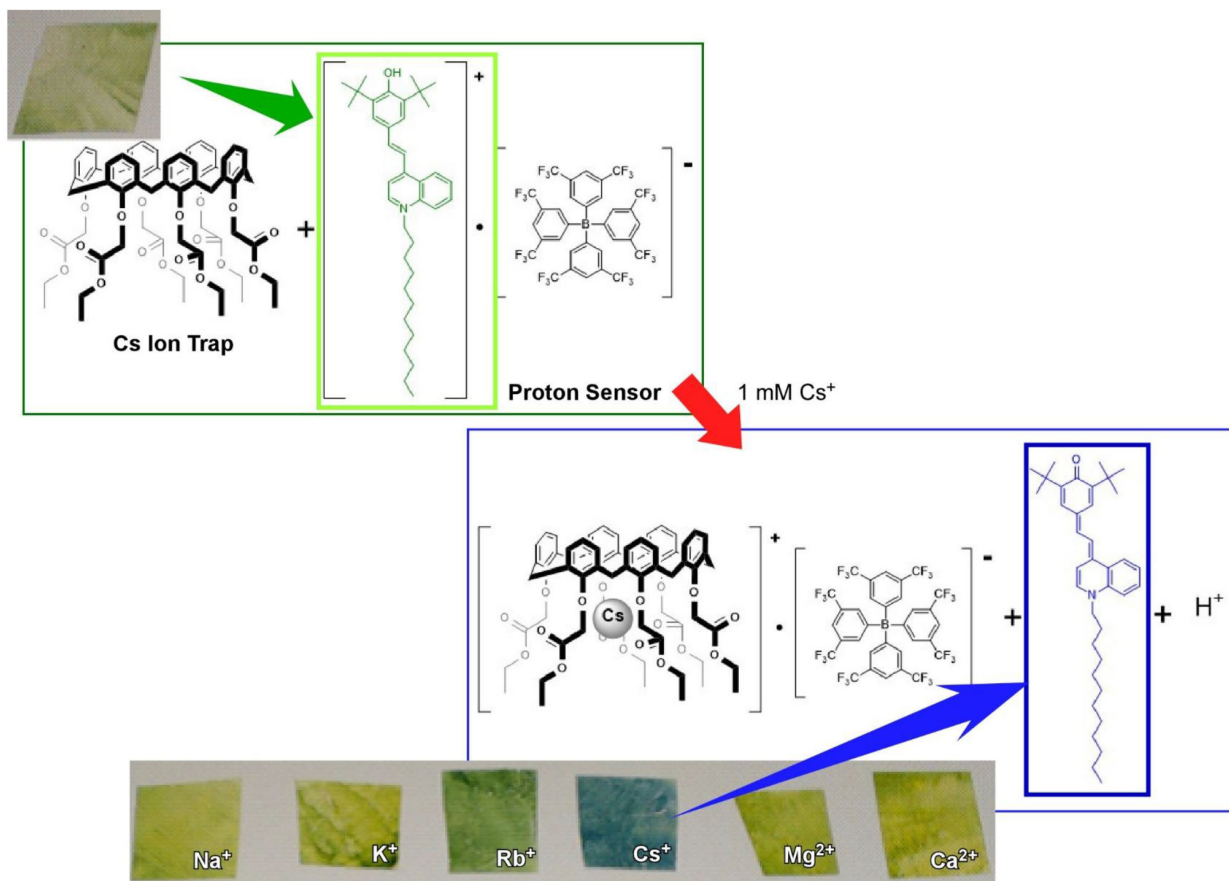


Figure 9. Supramolecular assembly of optode sensor system for detection of Cs ions in solution through color changes of the film.

tonics can convert abundant, ordinary materials into precious catalysts.^[100]

Typically, one of the major drawbacks of nanoparticle-type catalysts is particle agglomeration at higher temperature, which hinders catalytic capabilities. Rational design of catalyst morphology by considering nanoarchitectonic approaches has become a powerful approach to overcome agglomeration-related decreases in catalyst performance. In one example, micrometer-sized hollow Pt cells were synthesized via deposition of Pt metals on a polymer sphere template and the subsequent combustion of the template central polymer core (Figure 10).^[101] The latter process induced the formation of mouth-like holes on hollow Pt capsule surface. The fabricated mouth structure ensures the diffusion of reaction substrates into the Pt catalytic sites on the inner wall of the hollow capsules. Inside, the Pt catalytic sites are completely free from performance degradation by particle agglomeration. The fabricated open-mouth hollow capsules are called metallic cells. As a result, the catalytic performance for CO-remediation, namely $\text{CO} + 1/2\text{O}_2 \rightarrow \text{CO}_2$, of the hollow

metallic cells is significantly higher than that observed with conventional Pt particle catalysts due to the increase in the density of surface Pt sites per weight and avoiding agglomeration-related performance loss. Indeed, this strategy minimizes the use of Pt sources while achieving equivalent or superior catalytic performance and aiding the resource conservation of precious metals. Structural optimization, and the resulting gains in material usage efficiency, may also be applied to other applications involving precious elements, including rare metals.

Similarly, the sintering of catalytic nanoparticles often poses a serious impediment to achieve high catalytic performance. Sintering-resistant behaviors of precious catalysts can be achieved though maximizing the particle-to-particle separation distance between neighboring catalytic nanoparticles upon immobilizing them onto appropriate nanostructures.^[102] Catalytic Pt nanoparticles placed on wide-mouthed compartments that are fabricated on the surface of silica nanosheets exhibited maintenance of their particle size even after calcination at elevated temperatures. The sintering probability

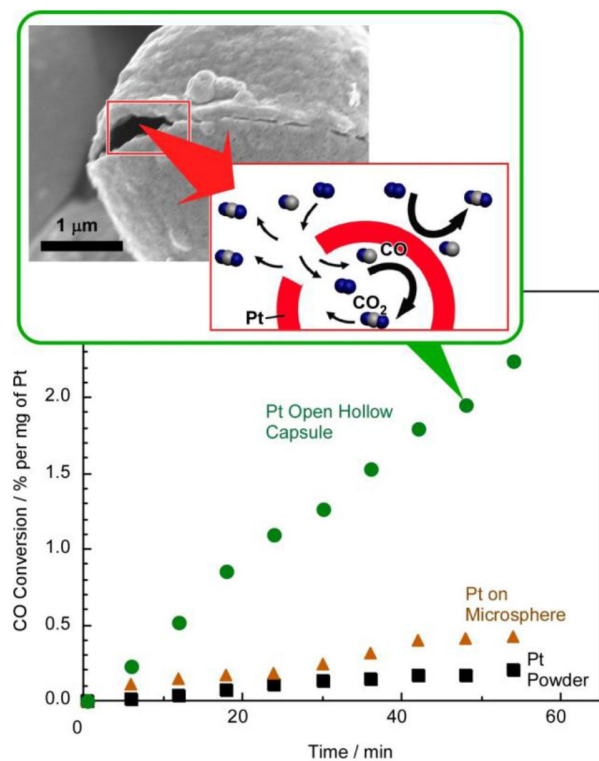


Figure 10. Micrometer-sized hollow Pt cells (metallic cells) for agglomeration-tolerant catalytic performance of CO remediation ($\text{CO} + 1/2\text{O}_2 \rightarrow \text{CO}_2$): green, metallic cell (Pt open hollow capsule); brown, Pt on microsphere; black, Pt powder.

was reduced upon the elongation of the particle-to-particle separation distance within the compartment structures, while the open-mouth structure ensures facile access of gas-phase reaction substances to the catalyst nanoparticles. The catalytic Pt nanoparticles immobilized on the wide-mouthed compartments possessed much higher activity for CO oxidation, as compared to the same Pt nanoparticles confined within the nanochannels of mesoporous silica. Strikingly, the obtained results demonstrate the importance of precisely controlling the dimensions of nanospace structures for developing effective green catalysts.

Nanoarchitectonic approaches to tune catalytically active lattices in materials structure can sometimes result in highly efficient catalysts derived from naturally abundant materials. The following example demonstrates that common CuO nanomaterials show high catalytic activities for NO remediation at levels that are comparable to those achieved by precious Rh catalysts and much higher than those achieved by Pt catalysts.^[103] This CuO-based catalyst was architected through a synthetic process at 140 °C using abundant materials of CuCl_2 , urea, and ethylene glycol. This procedure

provides CuO materials to prepare assembled crystalline nanosheets in a flower-like shape. The nanosheets primarily exhibit the {001} facet, as observed by high-resolution transition electron microscopy. The {001} facets have high activities for NO remediation, and exposure of the {001} facet was preserved in the integrated flower-shaped nanoarchitecture. Introduction of the flower-shaped CuO catalysts into actual engines resulted in NO remediation of real exhaust gases, and the NO concentration was quickly reduced. This example highlights how a nanoarchitectonic approach can preserve functionally active lattice structures while transforming common CuO into a high-performance material resembling precious Pt and Rh. Additionally, efficient control of the metallic atom composition with lattice engineering can modulate the catalytic of intermetallic TaPt_3 nanoparticles for realizing the electrooxidation of ethanol to CO_2 ^[104] and mixed-valence tin oxide, $(\text{Sn}^{2+})_2(\text{Sn}^{4+})\text{O}_4$, for photocatalytic hydrogen evolution from aqueous solutions.^[105]

3.5. Green Catalyst and Environmental Remediation: Nanospace Confinement

The confinement of catalysts within nano-sized spaces sometimes enhances certain aspects of catalyst performance such as efficiency, reaction selectivity, and stability. Mesoporous materials often provide media appropriate for enhanced catalytic performance. For example, gold nanoparticle catalysts can be trapped within mesoporous carbon nitride with the aid of the basic nature of carbon nitride.^[106] Interestingly, formation of gold nanoparticles within the mesoporous channels of carbon nitride does not require the use of any stabilizing, size-forming or reducing agent, and is possible under a single-step green condition. The confinement effect during the synthesis of gold nanoparticles leads to the preservation of active, ultra-small size catalysts. The fabricated gold nanoparticles exhibited high catalytic activity regarding the coupling reaction between benzaldehyde, piperidine, and phenyl acetylene.

As an interesting hollow nanomaterial for catalyst supports, the clay nanotube, halloysite, has received growing attention. Halloysite nanotubes have a hollow cylindrical shape with an SiO_x exterior and AlO_x interior, and are organic materials that are naturally abundant on the scale of thousands of tons.^[107] Selective immobilization of Cu^{2+} and Ni^{2+} cations to the cationic AlO_x interior together with anionic citrate has been achieved (Figure 11).^[108] Subsequent treatment with hydrazine converted the immobilized Cu^{2+} and Ni^{2+} cations into Cu–Ni nanoparticles. The fabricated Cu–Ni nanoparticles located in the interior of the halloysite nanotubes were used as catalysts for NO gas conversion. Because the agglomeration of Cu–Ni nanoparticles was prevented at the tube interior, the catalytic activities of the

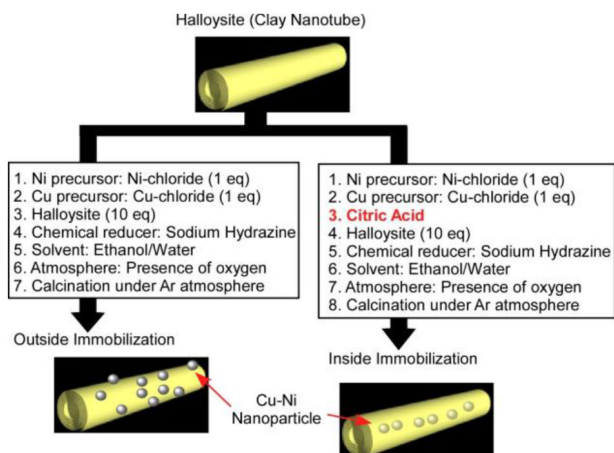


Figure 11. Selective immobilization of Cu–Ni nanoparticles onto the outside and inside of a Halloysite nanotube.

nanoparticles were maintained even at higher temperatures. By contrast, without the use of citrate in the immobilization process, the Cu–Ni nanoparticles were located on the external surface of the halloysite nanotubes. However, in the latter case, the catalytic activities of the nanoparticle at the exterior surface remained low. In addition, the interior immobilization of nanomaterials within halloysite nanotubes has been shown to facilitate antibacterial activity by immobilized silver nanorods within the halloysite nanotubes.^[109] Efficient suppression of bacterial growth was induced by the sustained release of Ag^+ ions from the functionalized interiors of the halloysite nanotubes.

Nanostructures are often regarded as useful platforms for trapping greenhouse gasses such as CO_2 .^[110] Rapid CO_2 exchange by carbonate anions intercalated within layered double hydroxide, which is a class of hydrotalcite, was recently demonstrated.^[111] The observed phenomenon revealed how naturally occurring nanostructures can have an unexpectedly large influence on the global carbon cycle. Some kinds of nanoarchitecture-inspired artificial structures such as metal-organic frameworks and/or coordination polymers are also capable of selective CO_2 capture.^[112] Metal-organic frameworks featuring fused Star-of-David catenanes have porous nanostructures with a two-fold intercatenated gyroid framework.^[113] The fabricated Star-of-David-type metal-organic frameworks exhibited highly selective CO_2 capture capabilities.

3.6. Bio-Friendly Applications

The nanoarchitectonics concept has also become an emerging design principle in the biological field.^[114] For the past few

years, nanoarchitectonics has received significant interest for biomedical applications, especially related to carbon and silicon materials. Applying nanoarchitectonics has opened a new door to solve difficult biological problems and advance fields such as bionanotechnology.

For example, various types of fullerene assemblies as novel nanoarchitectures have been used in the biological field. Two-dimensional assemblies of fullerene whiskers aligned at the air-water interface were demonstrated to be suitable platforms for regulated cell growth and cell differentiation (Figure 12).^[115] It has also been observed that neural stem cells on aligned C_{60} whiskers have a greater tendency to differentiate into mature neurons.^[116] It was thus suggested that aligned C_{60} whiskers may provide a functional scaffold for neural tissue engineering. Indeed, 2D materials provide a platform for cells to contact with plasmids for enhanced gene delivery. Following this approach, DNA transfection has been successfully achieved through the unique surface structure of nanosheets.^[117] In another study, silica upright nanosheets promoted naked DNA transfection into human mesenchymal stem cells without involving any transfection reagent.^[118] The critical physicochemical parameter of nanosheets that enables

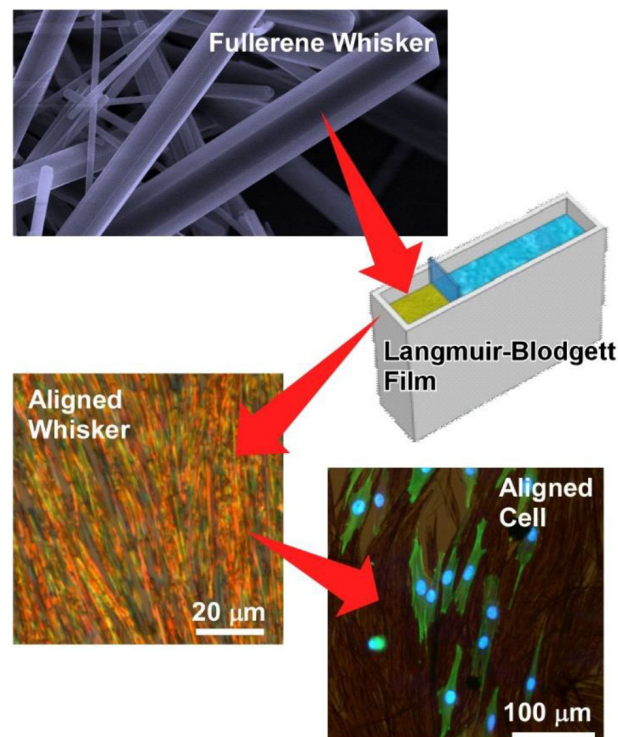


Figure 12. Two-dimensional assemblies of fullerene whiskers aligned at the air-water interface provide effective media conditions for regulating cell growth and cell differentiation.

effective delivery of DNA has been identified as the aspect ratio of the upright nanosheets.^[119]

The combination of carbon materials with other polymeric materials has also proven to be a feasible approach for various biomedical applications. Among the options, graphene, which is considered to have high biocompatibility, has become a frequent choice for biomedical applications such as drug delivery and tissue engineering.^[120] Graphene has been reported to promote the proliferation and differentiation of neural stem cells.^[121] When graphene was added to polymeric hydrogel, the nanocomposite hydrogel provided a new type of 3D printing ink and could be printed together with neural stem cells for nerve tissue engineering.^[122]

These biocompatible nanomaterials can possess nanostructure designs and, at the same time, further assemble into higher-order dimensions and/or complex materials to match cellular dimensions for functional uses such as inducing cellular responses. The techniques of nanoarchitectonics can be used to control nanoscale structures and spaces for various tissue engineering purposes. Moreover, in combination with other soft materials, nanomaterials can be applied in different forms, sizes, and properties. They may also retain their sensing functions to add value to a wide range of applications. Through their versatile implementation, nanoarchitectonic materials have emerged as highly capable materials for biological and medical applications.

Nanoarchitecture-based structures have been used for the delicate separation of materials in highly important biomedical applications. For example, technetium-99 m (^{99m}Tc) is an important nuclear element for various diagnostic applications, including tumor imaging, bone scans, cardiac perfusion, brain perfusion, and single photon emission computed tomography imaging. Efficient separation of ^{99m}Tc from $^{99}\text{Mo}/^{99m}\text{Tc}$ generators, which adsorb to metal oxide surfaces such as alumina, is crucial. Materials that promote strong Mo adsorption is useful for their efficient separation. Enhancing the surface area and pore volume through nanoarchitecture-based design of aluminum materials into mesoporous alumina with changing preparative conditions such as varying calcination temperatures, resulted in increased adsorption of Mo (41.6 mg g^{-1}) compared to that of commercial alumina powder (34.9 mg g^{-1}).^[123] Increased Mo adsorption was also observed for alumina-embedded mesoporous silica, which was prepared through the introduction of aluminum butoxide into silica mesopores and subsequent conversion to alumina at high temperatures.^[124] The presence of Lewis acid sites within the optimized mesoporous structures could enhance the adsorption of Mo species.

Nanoarchitectonic efforts can continuously improve Mo adsorption capacity, especially when integrated with other chemical-based approaches. A post-synthesis treatment step, involving, water-ethanol exposure, to process aluminium

glycerate nanospheres prepared by calcination at high temperature resulted in the formation of mesoporous aluminum nanosphere materials with superior dimensions such as high surface area and narrow pore size distribution.^[125] The prepared materials have distinct features, including lower crystallization temperature, that is advantageous for formation of the $\gamma\text{-Al}_2\text{O}_3$ phase. These structural features enable the newly fabricated materials to exhibit 2–10 times greater Mo adsorption capacity than those observed for similar materials without any post-treatment step. Further optimization of the materials through doping or composite designs with oxides possessing Lewis acid sites would create nanoarchitecture-inspired materials that are useful as $^{99}\text{Mo}/^{99m}\text{Tc}$ generators for diagnostic nuclear medicine.

4. Perspectives

Green operations with energy-efficient resource/waste-efficient, and bio-friendly processes can be realized through the rational design of highly sophisticated nanostructures with atomic/molecular/nano-level structural precisions. In order to accomplish different kinds of environmentally green processes such as bioprocessing and drug delivery, precious-metal-less catalysts, and environmental remediation, the well-considered structural formation of functional material units based on the nanoarchitectonics concept is vital. This account article presented various examples that were mainly classified according to membrane platforms and nanomaterial platforms, with examples presented across many types of applications such as sensing, catalysis, environmental remediation, and bio-interactions. Features of the presented examples can be classified based on different aspects of nanoarchitectonic control: (i) lattice and elemental composition (catalysts with non-precious metals); (ii) microscopic structural controls to avoid unfavorable structural damages (hollow capsule and metallic cell); (iii) high surface area for promoting interaction (mesoporous materials and self-assembled structures); (iv) biomimetic structures for better interaction with bio-targets (supported lipid bilayer membranes); (v) controlled layered structure for sequential action (layer-by-layer reactor); (vi) confinement effects to isolate active sites (mesoporous materials and clay nanotubes).

These examples highlight how nanostructured interfaces play crucial roles in enhancing molecular interactions and optimizing functional performance. Interfacial nanoarchitectonics is surely an important subject to design and fabricate functional materials.^[126] However, the role of interfaces is not limited to providing facile contacts between interactive species. Interfaces can also convert environmental-friendly mechanical motions into molecular level function.^[127] In particular, interfacial environments with many motional degrees of freedom such as the air-water interface can be

regarded as media appropriate for connecting macroscopic mechanical motions (lateral direction) and molecular functions (thickness direction). For example, molecular machines located at the air-water interface can be operated by macroscopic motions of lateral compression and expansion of interfacial films (Figure 13).^[128] Reversible capture and release of target molecules by molecular machines^[129] and mechanical tuning of molecular receptors for optimal guest discrimination^[130] can be accomplished through the environmentally friendly process of hand-motion-like mechanical actions. Theoretical calculations and thermodynamic analyses further demonstrated that molecular controls by macroscopic mechanical motions are highly energy efficient.^[131] Hand motion is regarded as one of the most opportune actions for operating molecular machines and molecular receptors among various stimuli such as light irradiation and redox control.

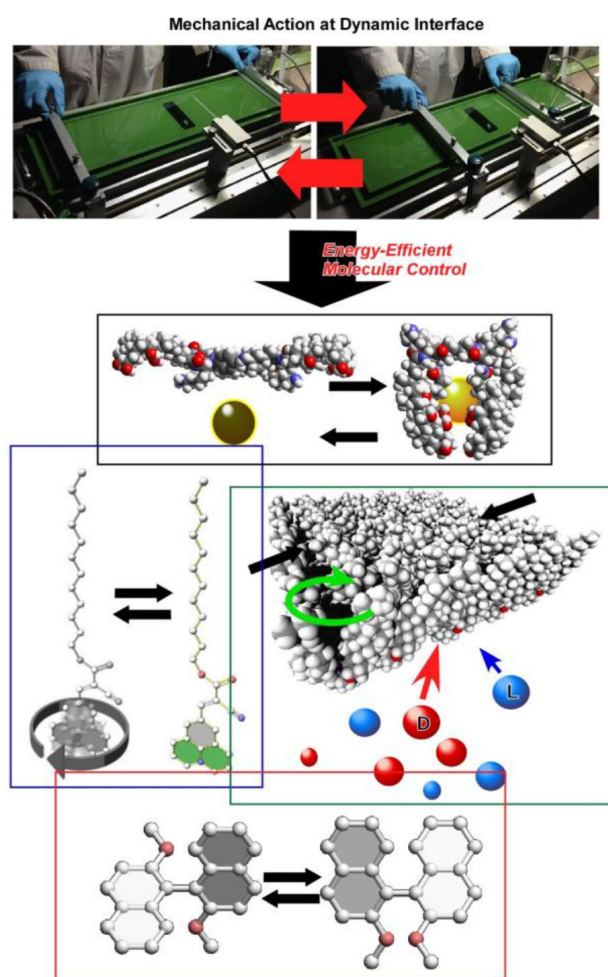


Figure 13. Various molecular machines embedded at the air-water interface can be operated by macroscopic energy-efficient hand-like motions.

Controls by the hand motions efficiently induce operation of countless numbers of molecular machines and related molecular systems together in synchronized ways, and are sometimes useful for unusual organization of molecular systems such as supramolecular polymerization of DNA origami pieces.^[132] These efficient systems can be fabricated through a well-designed nanoarchitectonic approach in the two-dimensional plane, the so-called interfacial environment. In another example, highly organized two-dimensional nanoarchitectures of organic semiconductors^[133] are expected to drastically reduce the operating voltage of display devices and in turn minimize production costs, leading to green-manufacturing of electronic devices.

By highlighting the unique roles that interfacial environments play in achieving efficient control over molecular processes, examples described in this account article demonstrate the importance of logical design and nanostructure-level fabrication for energy-efficient, resource/waste-efficient, and bio-friendly processes. Such aspects may not be well-covered by the conventional nanotechnology concept alone. To expand the conceptual space and inspire new innovations in application-oriented scientific research, methodology based on the nanoarchitectonics concept, including nanostructure control and organization to higher levels, is crucial and will create efficient and environmentally friendly systems. Looking forward, nanoarchitectonics will play an important role in future green chemistry.

Acknowledgements

This study was partially supported by JSPS KAKENHI Grant Number JP16H06518 (Coordination Asymmetry) and CREST JST Grant Number JPMJCR1665.

References

- [1] a) S. D. Stranks, H. J. Snaith, *Nat. Nanotechnol.* **2015**, *10*, 391–402; b) D. M. Cate, J. A. Adkins, J. Mettakoonpitak, C. S. Henry, *Anal. Chem.* **2015**, *87*, 19–41; c) S. Stauss, I. Honma, *Bull. Chem. Soc. Jpn.* **2018**, *91*, 492–505; d) R. K. Ulaganathan, Y.-H. Chang, D.-Y. Wang, S.-S. Li, *Bull. Chem. Soc. Jpn.* **2018**, *91*, 761–771.
- [2] a) N. A. Romero, D. A. Nicewicz, *Chem. Rev.* **2016**, *116*, 10075–10166; b) S. Matsubara, *Bull. Chem. Soc. Jpn.* **2018**, *91*, 82–86; c) K. Tanaka, *Bull. Chem. Soc. Jpn.* **2018**, *91*, 187–194.
- [3] a) W. Chaikittisilp, N. L. Torad, C. Li, M. Imura, N. Suzuki, S. Ishihara, K. Ariga, Y. Yamauchi, *Chem. Eur. J.* **2014**, *20*, 4217–4221; b) D. Larcher, J.-M. Tarascon, *Nat. Chem.* **2015**, *7*, 19–29; c) P. Song, Y. Li, F. Ma, T. Pullerits, M. Sun, *Chem. Rec.* **2016**, *16*, 734–753; d) C. Sengottaiyan, R. Jayavel, P. Bairi, R. G. Shrestha, K. Ariga, L. K. Shrestha, *Bull. Chem. Soc. Jpn.* **2017**, *90*, 955–962; e) Y. Yamada, T.

- Yamada, Y. Kanemitsu, *Bull. Chem. Soc. Jpn.* **2017**, *90*, 1129–1140; f) M. Irie, M. Morimoto, *Bull. Chem. Soc. Jpn.* **2018**, *91*, 237–250; g) Y. Kobayashi, *Bull. Chem. Soc. Jpn.* **2018**, *91*, 467–485.
- [4] a) X. Liu, L. Dai, *Nat. Rev. Mater.* **2016**, *1*, 16064; b) Z. Li, S. Wu, W. Lv, J.-J. Shao, F. Kang, Q.-H. Yang, *Small* **2016**, *12*, 2674–2688; c) M. Gon, K. Tanaka, Y. Chujo, *Bull. Chem. Soc. Jpn.* **2017**, *90*, 463–474.
- [5] a) E. Blanco, H. Shen, M. Ferrari, *Nat. Biotechnol.* **2015**, *33*, 941–951; b) A. A. Tahir, H. Ullah, P. Sudhagar, M. A. M. Teridi, A. Devadoss, S. Sundaram, *Chem. Rec.* **2016**, *16*, 1591–1634; c) Y. Katayama, *Bull. Chem. Soc. Jpn.* **2017**, *90*, 12–21; d) T. Morii, *Bull. Chem. Soc. Jpn.* **2017**, *90*, 1309–1317.
- [6] a) D. Larcher, J.-M. Tarascon, *Nat. Chem.* **2015**, *7*, 19–29; b) K. Motokura, *Bull. Chem. Soc. Jpn.* **2017**, *90*, 137–147; c) J. Yamaguchi, K. Itami, *Bull. Chem. Soc. Jpn.* **2017**, *90*, 367–383.
- [7] a) V. K. Sharma, L. Chen, R. Zboril, *ACS Sus. Chem. Eng.* **2016**, *4*, 18–34; b) K. Takimiya, M. Nakano, *Bull. Chem. Soc. Jpn.* **2018**, *91*, 121–140; c) M. Li, S. Kang, J. Du, J. Zhang, J. Wang, K. Ariga, *Angew. Chem. Int. Ed.* **2018**, *57*, 4936–4939; *Angew. Chem.* **2018**, *130*, 5030–5033; d) N. Chatani, *Bull. Chem. Soc. Jpn.* **2018**, *91*, 211–222; e) S. Hiroto, *Bull. Chem. Soc. Jpn.* **2018**, *91*, 829–838.
- [8] a) W. Chaikittisilp, K. Ariga, Y. Yamauchi, *J. Mater. Chem. A* **2013**, *1*, 14–19; b) N. L. Torad, M. Hu, S. Ishihara, H. Sukegawa, A. Belik, M. Imura, K. Ariga, Y. Sakka, Y. Yamauchi, *Small* **2014**, *10*, 2096–2107; c) S. L. Suib, *Chem. Rec.* **2017**, *17*, 1169–1183.
- [9] a) K. Ariga, J. P. Hill, M. V. Lee, A. Vinu, R. Charvet, S. Acharya, *Sci. Technol. Adv. Mater.* **2008**, *9*, 014109; b) C. Putta, V. Sharavath, S. Sarkar, S. Ghosh, *RSC Adv.* **2015**, *5*, 6652–6660; c) T. Shimizu, *Bull. Chem. Soc. Jpn.* **2018**, *91*, 623–668; d) Y. Haketa, H. Maeda, *Bull. Chem. Soc. Jpn.* **2018**, *91*, 420–436.
- [10] a) E. Ruiz-Hitzky, M. Darder, P. Aranda, K. Ariga, *Adv. Mater.* **2010**, *22*, 323–336; b) H. Zhu, W. Luo, P. N. Ciesielski, Z. Fang, J. Y. Zhu, G. Henriksson, M. E. Himmel, L. Hu, *Chem. Rev.* **2016**, *116*, 9305–9374; c) K. Minami, T. Mori, W. Nakanishi, N. Shigi, J. Nakanishi, J. P. Hill, M. Komiyama, K. Ariga, *ACS Appl. Mater. Interfaces* **2017**, *9*, 30553–30560; d) T. Sawada, T. Serizawa, *Bull. Chem. Soc. Jpn.* **2018**, *91*, 455–466.
- [11] a) Y. Qiang, S. Zhang, L. Guo, X. Zheng, B. Xiang, S. Chen, *Corros. Sci.* **2017**, *119*, 68–78; b) T. Taniguchi, *Bull. Chem. Soc. Jpn.* **2017**, *90*, 1005–1016; c) J. Aihara, *Bull. Chem. Soc. Jpn.* **2018**, *91*, 274–303; d) N. Yoshinari, T. Konno, *Bull. Chem. Soc. Jpn.* **2018**, *91*, 790–812; e) S. Dhiman, S. J. George, *Bull. Chem. Soc. Jpn.* **2018**, *91*, 687–699.
- [12] a) D. Nath, P. Banerjee, *Environ. Toxicol. Pharmacol.* **2013**, *36*, 997–1014; b) M. E. Vance, T. Kuiken, E. P. Vejerano, S. P. McGinnis, M. F. Hochella, Jr., D. Rejeski, M. S. Hull, *Beilstein J. Nanotechnol.* **2015**, *6*, 1769–1780; c) P. Formoso, R. Muzzalupo, L. Tavano, G. De Filipo, F. P. Nicoletta, *Mini-Rev. Med. Chem.* **2016**, *16*, 668–675.
- [13] a) Y.-J. Chen, B. Groves, R. A. Muscat, G. Seelig, *Nat. Nanotechnol.* **2015**, *10*, 748–760; b) Y.-G. Huang, Y. Shiota, S.-Q. Su, S.-Q. Wu, Z.-S. Yao, G.-L. Li, S. Kanegawa, S. Kang, T. Kamachi, K. Yoshizawa, K. Ariga, O. Sato, *Angew. Chem. Int. Ed.* **2016**, *55*, 14628–14632; *Angew. Chem.* **2016**, *128*, 14848–14852; c) M. Taniguchi, *Bull. Chem. Soc. Jpn.* **2017**, *90*, 1189–1210; d) W.-H. Soe, Y. Shirai, C. Durand, Y. Yonamine, K. Minami, X. Bouju, M. Kolmer, K. Ariga, C. Joachim, W. Nakanishi, *ACS Nano* **2017**, *11*, 10357–10365; e) M. Suda, *Bull. Chem. Soc. Jpn.* **2018**, *91*, 19–28.
- [14] a) K. Ariga, H. Ito, J. P. Hill, H. Tsukube, *Chem. Soc. Rev.* **2012**, *41*, 5800–5835; b) X. Du, J. Zhou, J. Shi, B. Xu, *Chem. Rev.* **2015**, *115*, 13165–13307; c) T. Sagami, S. Umemoto, Y. O. Tahara, M. Miyata, Y. Yonamine, D. Ishikawa, T. Mori, K. Ariga, H. Miyake, S. Shinoda, *Bull. Chem. Soc. Jpn.* **2017**, *90*, 739–735; d) S. Cherumukkil, B. Vedhanarayanan, G. Das, V. K. Praveen, A. Ajayaghosh, *Bull. Chem. Soc. Jpn.* **2018**, *91*, 100–120; f) S. Hiraoka, *Bull. Chem. Soc. Jpn.* **2018**, *91*, 957–978.
- [15] a) W. Nakanishi, K. Minami, L. K. Shrestha, Q. Ji, J. P. Hill, K. Ariga, *Nano Today* **2014**, *9*, 378–394; b) S. Wang, K. Li, Y. Chen, H. Chen, M. Ma, J. Feng, Q. Zhao, J. Shi, *Biomaterials* **2015**, *39*, 206–217; c) R. Sakamoto, *Bull. Chem. Soc. Jpn.* **2017**, *90*, 272–278; d) T. Mori, H. Tanaka, A. Dalui, N. Mitoma, K. Suzuki, M. Matsumoto, N. Aggarwal, A. Patnaik, S. Acharya, L. K. Shrestha, H. Sakamoto, K. Itami, K. Ariga, *Angew. Chem. Int. Ed.* **2018**, *57*, 9679–9683.
- [16] a) K. Ariga, Y. Yamauchi, M. Aono, *APL Mater.* **2015**, *3*, 061001; b) K. Ariga, Q. Ji, W. Nakanishi, J. P. Hill, M. Aono, *Mater. Horiz.* **2015**, *2*, 406–413; c) K. Ariga, K. Minami, M. Ebara, J. Nakanishi, *Polym. J.* **2016**, *48*, 371–389.
- [17] a) K. Ariga, Q. Ji, J. P. Hill, Y. Bando, M. Aono, *NPG Asia Mater.* **2012**, *4*, e17; b) K. Ariga, M. Aono, *Jpn. J. Appl. Phys.* **2016**, *55*, 1102 A6.
- [18] a) K. Ariga, M. Li, G. J. Richards, J. P. Hill, *J. Nanosci. Nanotechnol.* **2011**, *11*, 1–13; b) K. Ariga, J. Li, J. Fei, Q. Ji, J. P. Hill, *Adv. Mater.* **2016**, *28*, 1251–1286.
- [19] a) M. Aono, K. Ariga, *Adv. Mater.* **2016**, *28*, 989–992; b) K. Ariga, *Mater. Chem. Front.* **2017**, *1*, 208–211.
- [20] a) L. K. Shrestha, T. Mori, K. Ariga, *Curr. Opin. Colloid Interface Sci.* **2018**, *35*, 68–80; b) A. Lorenzo, W. A. Marmisolle, E. M. Maza, M. Ceolin, O. Azzaroni, *Phys. Chem. Chem. Phys.* **2018**, *20*, 7570–7578.
- [21] a) Y. Wakayama, *Jpn. J. Appl. Phys.* **2016**, *55*, 1102AA; b) A. Nayak, S. Unayama, S. Tai, T. Tsuruoka, R. Waser, M. Aono, I. Valov, T. Hasegawa, *Adv. Mater.* **2018**, *30*, 1703261; c) Y. Yan, J. Ye, K. Wang, J. Yao, Y. S. Zhao, *Small* **2018**, *14*, 1702698.
- [22] a) M. Ramanathan, L. K. Shrestha, T. Mori, Q. Ji, J. P. Hill, K. Ariga, *Phys. Chem. Chem. Phys.* **2013**, *15*, 10580–10611; b) M. Ramanathan, K. Hong, Q. Ji, Y. Yonamine, J. P. Hill, K. Ariga, *J. Nanosci. Nanotechnol.* **2014**, *14*, 390–401; c) L. K. Shrestha, K. M. Strzelczyk, R. G. Shrestha, K. Ichikawa, K. Aramaki, J. P. Hill, K. Ariga, *Nanotechnology* **2015**, *26*, 204002; d) L. Zhang, T. Wang, Z. Shen, M. Liu, *Adv. Mater.* **2016**, *28*, 1044–1059; e) L. K. Shrestha, R. G.

- Shrestha, J. P. Hill, T. Tsuruoka, Q. Ji, T. Nishimura, K. Ariga, *Langmuir* **2016**, *21*, 12511–12519; f) M. Osada, T. Sasaki, *Dalton Trans.* **2018**, *47*, 2841–2851.
- [23] a) H. Abe, J. Liu, K. Ariga, *Mater. Today* **2016**, *19*, 12–18; b) Gonzalo E. Fenoy, E. Maza, E. Zelaya, W. A. Marmisollé, O. Azzaroni, *Appl. Surf. Sci.* **2017**, *416*, 24–32.
- [24] a) S. Ishihara, J. Labuta, W. Van Rossom, D. Ishikawa, K. Minami, J. P. Hill, K. Ariga, *Phys. Chem. Chem. Phys.* **2014**, *16*, 9713–9746; b) K. Ariga, K. Minami, L. K. Shrestha, *Analyst* **2016**, *141*, 2629–2638; c) M. Komiyama, T. Mori, K. Ariga, *Bull. Chem. Soc. Jpn.* **2018**, *91*, 1075–1111..
- [25] a) K. Ariga, S. Ishihara, H. Abe, M. Li, J. P. Hill, *J. Mater. Chem.* **2012**, *22*, 2369–2377; b) R. Rajendran, L. K. Shrestha, K. Minami, M. Subramanian, R. Jayavel, K. Ariga, *J. Mater. Chem. A* **2014**, *2*, 18480–18487; c) R. Rajendran, L. K. Shrestha, R. M. Kumar, R. Jayavel, J. P. Hill, K. Ariga, *J. Inorg. Organomet. Polym. Mater.* **2015**, *25*, 267–274; d) Q. Zou, K. Liu, M. Abbas, X. Yan, *Adv. Mater.* **2016**, *28*, 1031–1043; e) J. Kim, J. H. Kim, K. Ariga, *Joule* **2017**, *1*, 739–768..
- [26] a) K. Ariga, M. V. Lee, T. Mori, X.-Y. Yu, J. P. Hill, *Adv. Colloid Interface Sci.* **2010**, *154*, 20–29; b) K. Ariga, K. Kawakami, M. Ebara, Y. Kotsuchibashi, Q. Ji, J. P. Hill, *New J. Chem.* **2014**, *38*, 5149–5163; c) K. Ariga, M. Naito, Q. Ji, D. Payra, *CrystEngComm* **2016**, *18*, 4890–4899; d) K. Ariga, *Anal. Sci.* **2016**, *32*, 1141–1149; e) K. Ariga, D. T. Leong, T. Mori, *Adv. Funct. Mater.* **2018**, *27*, 1702905.
- [27] a) L. K. Shrestha, R. G. Shrestha, S. Joshi, R. Rajbhandari, N. Shrestha, M. P. Adhikari, R. R. Pradhananga, K. Ariga, *J. Inorg. Organomet. Polym. Mater.* **2017**, *27*, S48–S56; b) E. Stulz, *Acc. Chem. Res.* **2017**, *50*, 823–831; c) M. Kryuchkova, R. Fakhruллин, *Environ. Sci. Technol. Lett.* **2018**, *5*, 295–300.
- [28] a) T. Mori, K. Sakakibara, H. Endo, M. Akada, K. Okamoto, A. Shundo, M. V. Lee, Q. Ji, T. Fujisawa, K. Oka, M. Matsumoto, H. Sakai, M. Abe, J. P. Hill, K. Ariga, *Langmuir* **2013**, *29*, 7239–7248; b) K. Ariga, T. Mori, J. P. Hill, *Langmuir* **2013**, *29*, 8459–8471; c) K. Ariga, T. Mori, J. Li, *Langmuir*, in press. DOI: 10.1021/acs.langmuir.8b01434
- [29] a) K. Ariga, T. Nakanishi, T. Michinobu, *J. Nanosci. Nanotechnol.* **2006**, *6*, 2278–2301; b) S. Casalini, C. A. Bortolotti, F. Leonardi, F. Biscarini, *Chem. Soc. Rev.* **2017**, *46*, 40–71.
- [30] a) S. Acharya, J. P. Hill, K. Ariga, *Adv. Mater.* **2009**, *21*, 2959–2981; b) K. Ariga, Y. Yamauchi, T. Mori, J. P. Hill, *Adv. Mater.* **2013**, *25*, 6477–6512; c) M. Iizuka, Y. Nakagawa, Y. Moriyama, E. Satou, A. Fujimori, *Bull. Chem. Soc. Jpn.* **2018**, *91*, 813–823.
- [31] a) K. Ariga, J. P. Hill, Q. Ji, *Phys. Chem. Chem. Phys.* **2007**, *9*, 2319–2340; b) K. Ariga, Y. Yamauchi, G. Rydzek, Q. Ji, Y. Yonamine, K. C.-W. Wu, J. P. Hill, *Chem. Lett.* **2014**, *43*, 36–68; c) G. Rydzek, Q. Ji, M. Li, P. Schaaf, J. P. Hill, F. Boulmedais, K. Ariga, *Nano Today* **2015**, *10*, 138–167.
- [32] a) X. Ling, Y.-H. Lee, Y. Lin, W. Fang, L. Yu, M. S. Dresselhaus, J. Kong, *Nano Lett.* **2014**, *14*, 464–472; b) W. Choi, N. Choudhary, G. H. Han, J. Park, D. Akinwande, Y. H. Lee, *Mater. Today* **2017**, *20*, 116–130.
- [33] a) J. J. Park, W. J. Hyun, S. C. Mun, Y. T. Park, O. O. Park, *ACS Appl. Mater. Interfaces* **2015**, *7*, 6317–6324; b) N. De Acha, C. Elosua, I. Matias, F. J. Arregui, *Sensors* **2017**, *17*, 2826; c) V. C. Rodrigues, M. L. Moraes, J. C. Soares, A. C. Soares, R. Sanfelice, E. Deffune, O. N. Oliveira, Jr., *Bull. Chem. Soc. Jpn.* **2018**, *91*, 891–896
- [34] a) C. Tan, X. Cao, X.-J. Wu, Q. He, J. Yang, X. Zhang, J. Chen, W. Zhao, S. Han, G.-H. Nam, M. Sindoro, H. Zhang, *Chem. Rev.* **2017**, *117*, 6225–6331; b) A. H. Khan, S. Ghosh, B. Pradhan, A. Dalui, L. K. Shrestha, S. Acharya, K. Ariga, *Bull. Chem. Soc. Jpn.* **2017**, *90*, 627–648; c) T. Low, A. Chaves, J. D. Caldwell, A. Kumar, N. X. Fang, P. Avouris, T. F. Heinz, F. Guinea, L. Martin-Moreno, F. Koppens, *Nat. Mater.* **2017**, *16*, 182–194; d) Z. Sarikhani, M. Manoochehri, *Bull. Chem. Soc. Jpn.* **2017**, *90*, 746–753; e) Y. Wang, C. C. Mayorga-Martinez, M. Pumera, *Bull. Chem. Soc. Jpn.* **2017**, *90*, 847–853
- [35] Q. Ji, I. Honma, S.-M. Paek, M. Akada, J. P. Hill, A. Vinu, K. Ariga, *Angew. Chem. Int. Ed.* **2010**, *49*, 9737–9739; *Angew. Chem.* **2010**, *122*, 9931–9933.
- [36] a) K. S. Lakhi, D.-H. Park, K. Al-Bahily, W. Cha, B. Viswanathan, J.-H. Choy, A. Vinu, *Chem. Soc. Rev.* **2017**, *46*, 72–101; b) Z. Qiu, J. Shu, D. Tang, *Anal. Chem.* **2017**, *89*, 5152–5160.
- [37] a) W. Shi, A. K. Friedman, L. A. Baker, *Anal. Chem.* **2017**, *89*, 157–188; b) R. R. Salunkhe, Y. V. Kaneti, Y. Yamauchi, *ACS Nano* **2017**, *11*, 5293–5308.
- [38] a) W. P. Lustig, S. Mukherjee, N. D. Rudd, A. V. Desai, J. Li, S. K. Ghosh, *Chem. Soc. Rev.* **2017**, *46*, 3242–3285; b) I. Stassen, N. Burtch, A. Talin, P. Falcaro, M. Allendorf, R. Ameloot, *Chem. Soc. Rev.* **2017**, *46*, 3185–3241.
- [39] K. Ariga, V. Vinu, Q. Ji, O. Ohmori, J. P. Hill, S. Acharya, J. Koike, S. Shiratori, *Angew. Chem. Int. Ed.* **2008**, *47*, 7254–7257; *Angew. Chem.* **2008**, *120*, 7364–7367.
- [40] Q. Ji, S. B. Yoon, J. P. Hill, A. Vinu, J.-S. Yu, K. Ariga, *J. Am. Chem. Soc.* **2009**, *131*, 4220–4221.
- [41] Q. Ji, X. Qiao, X. Liu, H. Jia, J. S. Yu, K. Ariga, *Bull. Chem. Soc. Jpn.* **2018**, *91*, 391–397..
- [42] a) Q. Ji, M. Miyahara, J. P. Hill, S. Acharya, A. Vinu, S. B. Yoon, J.-S. Yu, K. Sakamoto, K. Ariga, *J. Am. Chem. Soc.* **2008**, *130*, 2376–2377; b) Q. Ji, S. Acharya, J. P. Hill, A. Vinu, S. B. Yoon, J.-S. Yu, K. Sakamoto, K. Ariga, *Adv. Funct. Mater.* **2009**, *19*, 1792–1799.
- [43] B. L. Li, M. Setyawati, L. Chen, J. Xie, K. Ariga, C.-T. Lim, S. Garaj, D. T. Leong, *ACS Appl. Mater. Interfaces* **2017**, *9*, 15286–15296.
- [44] a) Y. Lvov, K. Ariga, T. Kunitake, *Chem. Lett.* **1994**, 2323–2326; b) Y. Lvov, K. Ariga, I. Ichinose, T. Kunitake, *J. Am. Chem. Soc.* **1995**, *117*, 6117–6123; c) K. Ariga, Q. Ji, T. Mori, M. Naito, Y. Yamauchi, H. Abe, J. P. Hill, *Chem. Soc. Rev.* **2013**, *42*, 6322–6345.
- [45] a) M. Onda, Y. Lvov, K. Ariga, T. Kunitake, *J. Ferment. Bioeng.* **1996**, *82*, 502–506; b) M. Onda, Y. Lvov, K. Ariga, T. Kunitake, *Biotechnol. Bioeng.* **1996**, *51*, 163–167.
- [46] M. Onda, K. Ariga, T. Kunitake, *J. Biosci. Bioeng.* **1999**, *87*, 69–75.
- [47] a) Y. Okahata, T. Tsuruta, K. Ijiri, K. Ariga, *Langmuir* **1988**, *4*, 1373–1375; b) Y. Okahata, T. Tsuruta, K. Ijiri, K. Ariga, *Thin Solid Films* **1989**, *180*, 65–72.

- [48] H. Wang, S. Ishihara, K. Ariga, Y. Yamauchi, *J. Am. Chem. Soc.* **2012**, *134*, 10819–10821.
- [49] M. B. Zakaria, C. Li, Q. Ji, B. Jiang, S. Tominaka, Y. Ide, J. P. Hill, K. Ariga, Y. Yamauchi, *Angew. Chem. Int. Ed.* **2016**, *55*, 8428–8430.
- [50] a) G. J. Hardy, R. Nayak, S. Zauscher, *Curr. Opin. Colloid Interface Sci.* **2013**, *18*, 448–458; b) J. van Weerd, M. Karperien, P. Jonkheijm, *Adv. Healthcare Mater.* **2015**, *4*, 2743–2779; c) F. Mazur, M. Bally, B. Städler, R. Chandrawati, *Adv. Colloid Interface Sci.* **2017**, *249*, 88–99.
- [51] a) C. Keller, B. Kasemo, *Biophys. J.* **1998**, *75*, 1397–1402; b) E. Reimhult, F. Höök, B. Kasemo, *Langmuir* **2003**, *19*, 1681–1691.
- [52] F. Höök, B. Kasemo, M. Grunze, S. Zauscher, *ACS Nano* **2008**, *2*, 2428–2436.
- [53] a) N.-J. Cho, C. W. Frank, *Langmuir* **2010**, *26*, 15706–15710; b) N.-J. Cho, J. A. Jackman, M. Liu, C. W. Frank, *Langmuir* **2011**, *27*, 3739–3748.
- [54] J. A. Jackman, J.-H. Choi, V. P. Zhdanov, N.-J. Cho, *Langmuir* **2013**, *29*, 11375–11384.
- [55] J. A. Jackman, Z. Zhao, V. P. Zhdanov, C. W. Frank, N.-J. Cho, *Langmuir* **2014**, *30*, 2152–2160.
- [56] K. H. Biswas, J. A. Jackman, J. H. Park, J. T. Groves, N.-J. Cho, *Langmuir* **2018**, *34*, 1775–1782.
- [57] M. D. Mager, B. Almquist, N. A. Melosh, *Langmuir* **2008**, *24*, 12734–12737.
- [58] A. O. Hohner, M. P. C. David, J. O. Rädler, *Biointerphases* **2010**, *5*, 1–8.
- [59] S. R. Tabaei, J.-H. Choi, G. Haw Zan, V. P. Zhdanov, N.-J. Cho, *Langmuir* **2014**, *30*, 10363–10373.
- [60] S. R. Tabaei, J. A. Jackman, S.-O. Kim, V. P. Zhdanov, N.-J. Cho, *Langmuir* **2015**, *31*, 3125–3134.
- [61] a) M. C. Kim, J. J. J. Gillissen, S. R. Tabaei, V. P. Zhdanov, N.-J. Cho, *Phys. Chem. Chem. Phys.* **2015**, *17*, 31145–31151; b) J. J. J. Gillissen, S. R. Tabaei, N.-J. Cho, *Phys. Chem. Chem. Phys.* **2016**, *18*, 24157–24163.
- [62] S. R. Tabaei, J. A. Jackman, M.-C. Kim, S. Yorulmaz, S. Vafaei, N.-J. Cho, *J. Vis. Exp.* **2015**, e53073.
- [63] a) J. A. Jackman, S. R. Tabaei, Z. Zhao, S. Yorulmaz, N.-J. Cho, *ACS Appl. Mater. Interfaces* **2015**, *7*, 959–968; b) S. R. Tabaei, S. Vafaei, N.-J. Cho, *Phys. Chem. Chem. Phys.* **2015**, *17*, 11546–11552.
- [64] a) S. R. Tabaei, J. A. Jackman, S.-O. Kim, B. Liedberg, W. Knoll, A. N. Parikh, N.-J. Cho, *Langmuir* **2014**, *30*, 13345–13352; b) S. R. Tabaei, J. A. Jackman, B. Liedberg, A. N. Parikh, N.-J. Cho, *J. Am. Chem. Soc.* **2014**, *136*, 16962–16965.
- [65] G. J. Hardy, R. Nayak, S. M. Alam, J. G. Shapter, F. Heinrich, S. Zauscher, *J. Mater. Chem.* **2012**, *22*, 19506–19513.
- [66] a) R. Zeineldin, J. A. Last, A. L. Slade, L. K. Ista, P. Bisong, M. J. O'Brien, S. Brueck, D. Y. Sasaki, G. P. Lopez, *Langmuir* **2006**, *22*, 8163–8168; b) S. R. Tabaei, P. Jönsson, M. Brändén, F. Höök, *J. Struct. Biol.* **2009**, *168*, 200–206.
- [67] K. Morigaki, S. Kimura, K. Okada, T. Kawasaki, K. Kawasaki, *Langmuir* **2012**, *28*, 9649–9655.
- [68] K. Kolahdouzan, J. A. Jackman, B. K. Yoon, M. C. Kim, M. S. Johal, N.-J. Cho, *Langmuir* **2017**, *33*, 5052–5064.
- [69] a) I. Reviakine, F. F. Rossetti, A. N. Morozov, M. Textor, *J. Chem. Phys.* **2005**, *122*, 204711; b) I. Reviakine, M. Gallego, D. Johannsmann, E. Tellechea, *J. Chem. Phys.* **2012**, *136*, 02B615.
- [70] J. A. Jackman, G. H. Zan, Z. Zhao, N.-J. Cho, *Langmuir* **2014**, *30*, 5368–5372.
- [71] J. A. Jackman, S. Yorulmaz Avsar, A. R. Ferhan, D. Li, J. H. Park, V. P. Zhdanov, N.-J. Cho, *Anal. Chem.* **2017**, *89*, 1102–1109.
- [72] I. Reviakine, D. Johannsmann, R. P. Richter, *Anal. Chem.* **2011**, *83*, 8838–8848.
- [73] J. J. J. Gillissen, S. R. Tabaei, J. A. Jackman, N.-J. Cho, *Analyst* **2017**, *142*, 3370–3379.
- [74] J. J. J. Gillissen, J. A. Jackman, S. R. Tabaei, B. K. Yoon, N.-J. Cho, *Anal. Chem.* **2017**, *89*, 11711–11718.
- [75] J. J. J. Gillissen, S. R. Tabaei, J. A. Jackman, N.-J. Cho, *Langmuir* **2018**, *34*, 503–511.
- [76] J. J. J. Gillissen, J. A. Jackman, S. R. Tabaei, N.-J. Cho, *Anal. Chem.* **2018**, *90*, 2238–2245.
- [77] E. Tellechea, D. Johannsmann, N. F. Steinmetz, R. P. Richter, I. Reviakine, *Langmuir* **2009**, *25*, 5177–5184.
- [78] a) K. Ariga, A. Vinu, Y. Yamauchi, Q. Ji, J. P. Hill, *Bull. Chem. Soc. Jpn.* **2012**, *85*, 1–32; b) K. Ariga, Y. Yamauchi, Q. Ji, Y. Yonamine, J. P. Hill, *APL Mater.* **2014**, *2*, 030701; c) V. Malgras, Q. Ji, Y. Kamachi, T. Mori, F.-K. Shieh, K. C.-W. Wu, K. Ariga, Y. Yamauchi, *Bull. Chem. Soc. Jpn.* **2015**, *88*, 1171–1200.
- [79] M. Hu, J. Reboul, S. Furukawa, N. L. Torad, Q. Ji, P. Srinivasu, K. Ariga, S. Kitagawa, Y. Yamauchi, *J. Am. Chem. Soc.* **2012**, *134*, 2864–2867.
- [80] a) A. Vinu, K. Ariga, T. Mori, T. Nakanishi, S. Hishita, D. Golberg, Y. Bando, *Adv. Mater.* **2005**, *17*, 1648–1652; b) G. P. Mane, S. N. Talapaneni, C. Anand, S. Varghese, H. Iwai, Q. Ji, K. Ariga, T. Mori, A. Vinu, *Adv. Funct. Mater.* **2012**, *22*, 3596–3604.
- [81] G. P. Mane, D. S. Dhawale, C. Anand, K. Ariga, Q. Ji, M. A. Wahab, T. Mori, A. Vinu, *J. Mater. Chem. A* **2013**, *1*, 2913–2920.
- [82] L. Jia, G. Lawrence, V. V. Balasubramanian, G. Choi, J.-H. Choy, A. M. A. Ali, A. Elzatahry, K. Ariga, A. Vinu, *Chem. Eur. J.* **2015**, *21*, 697–703.
- [83] M. P. Adhikari, R. Adhikari, R. G. Shrestha, R. Rajendran, L. Adhikari, P. Bairi, R. R. Pradhananga, L. K. Shrestha, K. Ariga, *Bull. Chem. Soc. Jpn.* **2015**, *88*, 1108–1115.
- [84] L. K. Shrestha, L. Adhikari, R. G. Shrestha, M. P. Adhikari, R. Adhikari, J. P. Hill, R. R. Pradhananga, K. Ariga, *Sci. Technol. Adv. Mater.* **2016**, *17*, 483–492.
- [85] a) A. Vinu, M. Miyahara, V. Sivamurugan, T. Mori, K. Ariga, *J. Mater. Chem.* **2005**, *15*, 5122–5127; b) K. Ariga, A. Vinu, M. Miyahara, J. P. Hill, T. Mori, *J. Am. Chem. Soc.* **2007**, *129*, 11022–11023.
- [86] Y. Kosaki, H. Izawa, S. Ishihara, K. Kawakami, M. Sumita, Y. Tateyama, Q. Ji, V. Krishnan, S. Hishita, Y. Yamauchi, J. P. Hill, A. Vinu, S. Shiratori, K. Ariga, *ACS Appl. Mater. Interfaces* **2013**, *5*, 2930–2934.

- [87] G. Lawrence, P. Kalimuthu, M. Benzigar, K. J. Shelat, K. S. Lakhi, D.-H. Park, Q. Ji, K. Ariga, P. V. Bernhardt, A. Vinu, *Adv. Mater.* **2017**, *29*, 1702295.
- [88] a) W. Zhang, Y. Zhao, V. Malgras, Q. Ji, D. Jiang, R. Qi, K. Ariga, Y. Yamauchi, J. Liu, J.-S. Jiang, M. Hu, *Angew. Chem. Int. Ed.* **2016**, *55*, 8228–8234; *Angew. Chem.* **2016**, *128*, 8368–8374; b) K. Kikuchi, Y. Tatewaki, S. Okada, *Bull. Chem. Soc. Jpn.* **2017**, *90*, 298–305; c) K. Matsuura, *Bull. Chem. Soc. Jpn.* **2017**, *90*, 873–884; d) V. F. Korolovych, A. J. Erwin, A. Stryutsky, E. K. Mikan, V. V. Shevchenko, V. V. Tsukruk, *Bull. Chem. Soc. Jpn.* **2017**, *90*, 919–923; e) J. Sasaki, M. Suzuki, K. Hanabusa, *Bull. Chem. Soc. Jpn.* **2018**, *91*, 538–547
- [89] a) L. K. Shrestha, Q. Ji, T. Mori, K. Miyazawa, Y. Yamauchi, J. P. Hill, K. Ariga, *Chem. Asian J.* **2013**, *8*, 1662–1679; b) P. Bairi, K. Minami, J. P. Hill, W. Nakanishi, L. K. Shrestha, C. Liu, K. Harano, E. Nakamura, K. Ariga, *ACS Nano* **2016**, *10*, 8796–8802; c) P. Bairi, T. Tsuruoka, S. Acharya, Q. Ji, J. P. Hill, K. Ariga, Y. Yamauchi, L. K. Shrestha, *Mater. Horiz.* **2018**, *5*, 285–290.
- [90] a) L. K. Shrestha, R. G. Shrestha, Y. Yamauchi, J. P. Hill, T. Nishimura, K. Miyazawa, T. Kawai, S. Okada, K. Wakabayashi, K. Ariga, *Angew. Chem. Int. Ed.* **2015**, *54*, 951–955; *Angew. Chem.* **2015**, *127*, 965–969.
- [91] P. Bairi, K. Minami, W. Nakanishi, J. P. Hill, K. Ariga, L. K. Shrestha, *ACS Nano* **2016**, *10*, 6631–6637
- [92] P. Bairi, K. Minami, J. P. Hill, K. Ariga, L. K. Shrestha, *ACS Nano* **2017**, *11*, 7790–7796.
- [93] a) G. Yoshikawa, T. Akiyama, S. Gautsch, P. Vettiger, H. Rohrer, *Nano Lett.* **2011**, *11*, 1044–1048; b) J. A. Jackman, N.-J. Cho, M. Nishikawa, G. Yoshikawa, T. Mori, L. K. Shrestha, K. Ariga, *Chem. Asian J.*, in press. DOI: 10.1002/asia.201800935.
- [94] I. Osica, G. Imamura, K. Shiba, Q. Ji, L. K. Shrestha, J. P. Hill, K. J. Kurzydowski, G. Yoshikawa, K. Ariga, *ACS Appl. Mater. Interfaces* **2017**, *9*, 9945–9954.
- [95] I. Osica, A. F. A. A. Melo, G. Imamura, Q. Ji, J. P. Hill, F. N. Crespilho, K. J. Kurzydowski, G. Yoshikawa, K. Ariga, *J. Nanosci. Nanotechnol.* **2017**, *17*, 5908–5917.
- [96] T. Mori, M. Akamatsu, K. Okamoto, M. Sumita, Y. Tateyama, H. Sakai, J. P. Hill, M. Abe, K. Ariga, *Sci. Technol. Adv. Mater.* **2013**, *14*, 015002.
- [97] M. Akamatsu, H. Komatsu, T. Mori, E. Adams, R. Shin, H. Sakai, M. Abe, J. P. Hill, K. Ariga, *ACS Appl. Mater. Interfaces* **2014**, *6*, 8208–8211.
- [98] M. Akamatsu, H. Komatsu, A. Matsuda, T. Mori, W. Nakanishi, H. Sakai, J. P. Hill, K. Ariga, *Bull. Chem. Soc. Jpn.* **2017**, *90*, 678–683.
- [99] a) Q.-W. Song, Z.-H. Zhou, L.-N. He, *Green Chem.* **2017**, *19*, 3707–3728; b) H. Nagashima, *Bull. Chem. Soc. Jpn.* **2017**, *90*, 761–775; c) Y. Shu, J. Maruyama, S. Iwasaki, C. Li, Y. Shen, H. Uyama, *Bull. Chem. Soc. Jpn.* **2017**, *90*, 1058–1066; d) R. A. Sheldon, *Green Chem.* **2017**, *19*, 18–43; e) M. S. Ghasemzadeh, B. Akhlaghinia, *Bull. Chem. Soc. Jpn.* **2017**, *90*, 1119–1128; f) J. Artz, T. E. Müller, K. Thenert, J. Kleinekorte, R. Meys, A. Sternberg, A. Bardow, W. Leitner, *Chem. Rev.* **2018**, *118*, 434–504; g) H. Kobayashi, A. Fukuoka, *Bull. Chem. Soc. Jpn.* **2018**, *91*, 29–43; h) R. Rahmawati, Y. V. Kaneti, A. Taufiq, Sunaryono, B. Yulianto, Suyatman, Nugraha, D. Kurniadi, Md. S. A. Hossain, Y. Yamauchi, *Bull. Chem. Soc. Jpn.* **2018**, *91*, 311–317.
- [100] K. Ariga, S. Ishihara, H. Abe, *CrystEngComm*, **2016**, *18*, 6770–6778.
- [101] S. Mandal, M. Sathish, G. Saravanan, K. K. R. Datta, Q. Ji, J. P. Hill, H. Abe, I. Honma, K. Ariga, *J. Am. Chem. Soc.* **2010**, *132*, 14415–14417.
- [102] J. Liu, Q. Ji, T. Imai, K. Ariga, H. Abe, *Sci. Rep.* **2017**, *7*, 41773.
- [103] F. M. Auxilia, S. Ishihara, S. Mandal, T. Tanabe, G. Saravanan, G. V. Ramesh, N. Umezawa, T. Hara, Y. Xu, S. Hishita, Y. Yamauchi, D. Arivuoli, J. P. Hill, K. Ariga, H. Abe, *Adv. Mater.* **2014**, *26*, 4481–4485.
- [104] R. Kodiyath, G. V. Ramesh, E. Koudelkova, T. Tanabe, M. Ito, M. Manikandan, S. Ueda, T. Fujita, N. Umezawa, H. Noguchi, K. Ariga, H. Abe, *Energy Environ. Sci.* **2015**, *8*, 1685–1689.
- [105] M. Manikandan, T. Tanabe, P. Li, S. Ueda, G. V. Ramesh, R. Kodiyath, J. Wang, T. Hara, D. Arivuoli, S. Ishihara, K. Ariga, J. Ye, N. Umezawa, H. Abe, *ACS Appl. Mater. Interfaces* **2014**, *6*, 3790–3793.
- [106] K. K. R. Datta, B. V. S. Reddy, K. Ariga, A. Vinu, *Angew. Chem. Int. Ed.* **2010**, *49*, 5961–5965; *Angew. Chem.* **2010**, *122*, 6097–6101.
- [107] a) Y. M. Lvov, D. G. Shchukin, H. Möhwald, R. R. Price, *ACS Nano* **2008**, *2*, 814–820; b) V. A. Vinokurov, A. V. Stavitskaya, Y. A. Chudakov, E. V. Ivanov, L. K. Shrestha, K. Ariga, Y. A. Darrat, Y. M. Lvov, *Sci. Technol. Adv. Mater.* **2017**, *18*, 147–151.
- [108] L. J. Eva; L. K. Shrestha, Y. Lvov, J. P. Hill, K. Ariga, H. Abe, *J. Mater. Chem. A* **2015**, *3*, 6614–6619.
- [109] E. Abdullayev, K. Sakakibara, K. Okamoto, W. Wei, K. Ariga, Y. Lvov, *ACS Appl. Mater. Interfaces* **2011**, *3*, 4040–4046.
- [110] a) E. D. Bates, R. D. Mayton, I. Ntai, J. H. Davis, *J. Am. Chem. Soc.* **2002**, *124*, 926–927; b) G. T. Rochelle, *Science* **2009**, *325*, 1652–1654; c) D. M. D'Alessandro, B. Smit, J. R. Long, *Angew. Chem. Int. Ed.* **2010**, *49*, 6058–6082; *Angew. Chem.* **2010**, *122*, 6194–6219; d) K. Teranishi, A. Ishikawa, H. Sato, H. Nakai, *Bull. Chem. Soc. Jpn.* **2017**, *90*, 451–460; e) A. W. Sakti, Y. Nishimura, H. Sato, H. Nakai, *Bull. Chem. Soc. Jpn.* **2017**, *90*, 1230–1235
- [111] a) S. Ishihara, P. Sahoo, K. Deguchi, S. Ohki, M. Tansho, T. Shimizu, J. Labuta, J. P. Hill, K. Ariga, K. Watanabe, Y. Yamauchi, S. Suehara, N. Iyi, *J. Am. Chem. Soc.* **2013**, *135*, 18040–18043; b) P. Sahoo, S. Ishihara, K. Yamada, K. Deguchi, S. Ohki, M. Tansho, T. Shimizu, N. Eisaku, R. Sasai, J. Labuta, D. Ishikawa, J. P. Hill, K. Ariga, B. P. Bastakoti, Y. Yamauchi, I. Iyi, Nobuo *ACS Appl. Mater. Interfaces* **2014**, *6*, 18352–18359.
- [112] a) R. Banerjee, A. Phan, B. Wang, C. Knobler, H. Furukawa, M. O'Keeffe, O. M. Yaghi, *Science* **2008**, *319*, 939–943; b) Y.-G. Huang, Y. Shiota, M.-Y. Wu, S.-Q. Su, Z.-S. Yao, S. Kang, S. Kanegawa, G.-L. Li, S.-Q. Wu, T. Kamachi, K. Yoshizawa, K. Ariga, M.-C. Hong, O. Sato, *Nat. Commun.*

- 2016, 7, 11564; c) K. Adil, Y. Belmabkhout, R. S. Pillai, A. Cadiou, P. M. Bhatt, A. H. Assen, G. Maurin, M. Eddaoudi, *Chem. Soc. Rev.* **2017**, 46, 3402–3430; d) J. Yu, L.-H. Xie, J.-R. Li, Y. Ma, J. M. Seminario, P. B. Balbuena, *Chem. Rev.* **2017**, 117, 9674–9754.
- [113] Y.-G. Huang, S.-Q. Wu, W.-H. Deng, G. Xu, F.-L. Hu, J. P. Hill, W. Wei, S.-Q. Su, L. K. Shrestha, O. Sato, M.-Y. Wu, M.-C. Hong, K. Ariga, *Adv. Mater.* **2017**, 29, 1703301.
- [114] a) K. Ariga, Q. Ji, M. J. McShane, Y. M. Lvov, A. Vinu, J. P. Hill, *Chem. Mater.* **2012**, 24, 728–737; b) K. Ariga, *ChemNanoMat* **2016**, 2, 333–343; c) M. Komiyama, K. Yoshimoto, M. Sisido, K. Ariga, *Bull. Chem. Soc. Jpn.* **2017**, 90, 967–1004; d) K. Ariga, T. Mori, L. K. Shrestha, *Chem. Rec.* **2018**, 18, 676–695.
- [115] a) V. Krishnan, Y. Kasuya, Q. Ji, M. Sathish, L. K. Shrestha, S. Ishihara, K. Minami, H. Morita, T. Yamazaki, N. Hanagata, K. Miyazawa, S. Acharya, W. Nakanishi, J. P. Hill, K. Ariga, *ACS Appl. Mater. Interfaces* **2015**, 7, 15667–15673; b) K. Minami, Y. Kasuya, T. Yamazaki, Q. Ji, W. Nakanishi, J. P. Hill, H. Sakai, K. Ariga, *Adv. Mater.* **2015**, 27, 4020–4026.
- [116] F. Y. Hsieh, L. K. Shrestha, K. Ariga, S. Hsu, *Chem. Commun.* **2017**, 53, 11024–11027.
- [117] Q. Ji, T. Yamazaki, N. Hanagata, M. V. Lee, J. P. Hill, K. Ariga, *Chem. Commun.* **2012**, 48, 8496–8498.
- [118] N. C. Huang, Q. Ji, K. Ariga, S. Hsu, *NPG Asia Mater.* **2015**, 7, e184.
- [119] N. C. Huang, Q. Ji, T. Yamazaki, W. Nakanishi, N. Hanagata, K. Ariga, S. Hsu, *Phys. Chem. Chem. Phys.* **2015**, 17, 25455–25462.
- [120] S. Goenka, V. San, S. Sant, *J. Controlled Release.* **2014**, 173, 75–88.
- [121] O. N. Ruiz, K. A. S. Fernando, B. Wang, N. A. Brown, P. G. Luo, N. D. McNamara, M. Vangsness, Y. P. Sun, C. E. Bunker, *ACS Nano* **2011**, 5, 8100–8107.
- [122] C. T. Huang, L. K. Shrestha, K. Ariga, S. Hsu, *J. Mater. Chem. B* **2017**, 5, 8854–8864.
- [123] I. Saptiama, Y. V. Kaneti, Y. Suzuki, Y. Suzuki, K. Tsuchiya, T. Sakae, K. Takai, N. Fukumitsu, Z. A. Allothman, M. S. A. Hossain, K. Ariga, Y. Yamauchi, *Bull. Chem. Soc. Jpn.* **2017**, 90, 1174–1179.
- [124] I. Saptiama, Y. V. Kaneti, H. Oveisi, Y. Suzuki, K. Tsuchiya, K. Takai, T. Sakae, S. Pradhan, M. S. A. Hossain, N. Fukumitsu, K. Ariga, Y. Yamauchi, *Bull. Chem. Soc. Jpn.* **2018**, 91, 195–200.
- [125] I. Saptiama, Y. V. Kaneti, Y. Suzuki, K. Tsuchiya, N. Fukumitsu, T. Sakae, J. Kim, Y.-M. Kang, K. Ariga, Y. Yamauchi, *Small* **2018**, 14, 1800474.
- [126] a) K. Ariga, Q. Ji, W. Nakanishi, J. P. Hill, *J. Inorg. Organomet. Polym. Mater.* **2015**, 25, 466–479; b) K. Ariga, V. Malgras, Q. Ji, M. B. Zakaria, Y. Yamauchi, *Coord. Chem. Rev.* **2016**, 320–321, 139–152; c) M. Mukai, S. L. Regen, *Bull. Chem. Soc. Jpn.* **2017**, 90, 1083–1087; d) X. Liu, J. G. Riess, M. P. Kraft, *Bull. Chem. Soc. Jpn.* **2018**, 91, 846–857; e) T. Mori, H. Komatsu, N. Sakamoto, K. Suzuki, J. P. Hill, M. Matsumoto, H. Sakai, K. Ariga, W. Nakanishi, *Phys. Chem. Chem. Phys.* **2018**, 20, 3073–3078.
- [127] a) K. Ariga, T. Mori, J. P. Hill, *Adv. Mater.* **2012**, 24, 158–176; b) Y. Shirai, K. Minami, W. Nakanishi, Y. Yonamine, C. Joachim, K. Ariga, *Jpn. J. Appl. Phys.* **2016**, 55, 1102 A2; c) K. Ariga, T. Mori, W. Nakanishi, J. P. Hill, *Phys. Chem. Chem. Phys.* **2017**, 19, 23658–23676.
- [128] a) K. Ariga, S. Ishihara, H. Izawa, H. Xia, J. P. Hill, *Phys. Chem. Chem. Phys.* **2011**, 13, 4802–4811; b) K. Ariga, T. Mori, J. P. Hill, *Soft Matter* **2012**, 8, 15–20; c) K. Ariga, T. Mori, S. Ishihara, K. Kawakami, J. P. Hill, *Chem. Mater.* **2014**, 26, 519–532; d) K. Ariga, T. Mori, W. Nakanishi, *Chem. Asian J.* **2018**, 13, 1266–1278.
- [129] a) K. Ariga, Y. Terasaka, D. Sakai, H. Tsuji, J. Kikuchi, *J. Am. Chem. Soc.* **2000**, 122, 7835–7836; b) K. Ariga, T. Nakanishi, Y. Terasaka, H. Tsuji, D. Sakai, J. Kikuchi, *Langmuir* **2005**, 21, 976–981.
- [130] a) T. Michinobu, S. Shinoda, T. Nakanishi, J. P. Hill, K. Fujii, T. N. Player, H. Tsukube, K. Ariga, *J. Am. Chem. Soc.* **2006**, 128, 14478–14479; b) T. Mori, K. Okamoto, H. Endo, J. P. Hill, S. Shinoda, M. Matsukura, H. Tsukube, Y. Suzuki, Y. Kanekiyo, K. Ariga, *J. Am. Chem. Soc.* **2010**, 132, 12868–12870; c) K. Sakakibara, L. A. Joyce, T. Mori, T. Fujisawa, S. H. Shabbir, J. P. Hill, E. V. Anslyn, K. Ariga, *Angew. Chem. Int. Ed.* **2012**, 51, 9643–9646; *Angew. Chem.* **2012**, 124, 9781–9784.
- [131] a) D. Ishikawa, T. Mori, Y. Yonamine, W. Nakanishi, D. Cheung, J. P. Hill, K. Ariga, *Angew. Chem. Int. Ed.* **2015**, 54, 8988–8991; *Angew. Chem.* **2015**, 127, 9116–9119; b) K. Ariga, W. Nakanishi, *J. Synth. Org. Chem. Jpn.* **2017**, 75, 219–227.
- [132] Y. Yonamine, K. Cervantes-Salguero, K. Minami, I. Kawamata, W. Nakanishi, J. P. Hill, S. Murata, K. Ariga, *Phys. Chem. Chem. Phys.* **2016**, 18, 12576–12581.
- [133] a) A. Yamamura, S. Watanabe, M. Uno, M. Mitani, C. Mitsui, J. Tsurumi, N. Isahaya, Y. Kanaoka, T. Okamoto, J. Takeya, *Sci. Adv.* **2018**, 4, ea0575; b) K. Ariga, S. Watanabe, T. Mori, J. Takeya, *NPG Asia Mater.* **2018**, 10, 90–106.

Received: July 12, 2018

Accepted: August 30, 2018

Published online on September 19, 2018